Measurement 263 (2026) 120168

Contents lists available at ScienceDirect

Measurement

journal homepage: www.elsevier.com/locate/measurement

Investigating the influence of individual physical effects on dimensional measurement deviations using XCT simulations

Miroslav Yosifov [a,b,*], Thiago Linhares Fernandes [c], Filippo Zanini [c], Simone Carmignato [c], Jan De Beenhouwer [a], Jan Sijbers [a], Johann Kastner [b], Christoph Heinzl [d,e]

[a] imec-Vision Lab, Dept. of Physics, University of Antwerp, Universiteitsplein 1, Antwerpen, 2610, Belgium
[b] CT Research Group, University of Applied Sciences Upper Austria, Stelzhamerstrasse 23, Wels, 4600, Austria
[c] Department of Management and Engineering, University of Padova, Stradella San Nicola 3, Vicenza, 36100, Italy
[d] Faculty of Computer Science and Mathematics, University of Passau, Innstraße 43, Passau, 94032, Germany
[e] Division Development Center X-ray Technology, Fraunhofer Institute for Integrated Circuits IIS, Flugplatzstraße 75, Fürth, 90768, Germany

ARTICLE INFO

Keywords:
X-ray computed tomography
Dimensional measurement
Uncertainty
XCT metrology
X-ray simulation

ABSTRACT

This study investigates individual sources of measurement deviations associated with physical effects in X-ray computed tomography (XCT) imaging, including focal spot blur effect, detector modulation transfer function, Poisson-Gaussian noise, and virtual gain correction. Key parameters were modeled to reflect XCT device characteristics, such as X-ray tube properties as well as detector attributes. Using a calibrated object designed for XCT metrology, namely a hole plate, a series of experiments were conducted to reproduce real measurement setups in a virtual simulation environment. XCT scans are compared with simulated XCT data generated under various conditions, including different numbers of projections (120 and 1000) and with physical effects both enabled and disabled. Deviations for both real and simulated XCT were determined by measuring hole diameters and distances between cylinder holes and comparing these measurements to reference values from the calibrated object, allowing quantification of the impact of different physical effects on measurement accuracy. The analysis revealed that virtual gain correction and focal spot blur had the most significant impact on measurement accuracy, with deviations of 0.018 mm and 0.016 mm, while Poisson–Gaussian noise had a minor influence of about 0.008 mm. The simulation framework accurately replicates XCT behavior (SSIM = 0.9645 for a simulated 1000 projections) and isolates individual physical effects. This study provides insight into the relative contributions of different physical effects to measurement deviations in industrial XCT. The findings have shown potential to guide future efforts in improving measurement accuracy, estimating measurement uncertainty, and developing more realistic simulation tools for XCT metrology.

1. Introduction and motivation

X-ray Computed Tomography (XCT) is a powerful non-destructive testing (NDT) technique for detailed internal visualization of objects [1]. It is widely applied in materials characterization [2,3], manufacturing evaluation [4,5], and medical imaging [6]. It plays a key role in identifying features such as defects (e.g., pores, cracks, inclusions or reinforcements (e.g., fibers), demonstrating its versatility [7–9]. Recent work has also highlighted the growing role of XCT in the metrological evaluation of porosity, enabling quantitative assessment of pore morphology, distribution, and measurement uncertainty in additively manufactured components [10]. Further studies show advances in micro-CT for material characterization [11,12], robust analysis at low resolutions [13], and deep learning-based pore segmentation [14]. To support visual analysis and enhance interpretation of XCT data, visualization tools such as open_iA [15] by Fröhler et al. or dedicated techniques for comparative visualization such as AccuStripes by Heim et al. [16] have been proposed to compare multiple XCT volumes.

X-ray simulation further extends the capabilities of XCT by providing a controlled environment for generating synthetic data, which addresses some of the challenges and limitations encountered in real-world XCT applications. It has demonstrated its capability in generating synthetic XCT data [17], improving on the defect detectability and enabling precise control over defect characteristics such as shape and size, as well as overall image quality [18]. It offers full control over the synthetic data generation process and supports the optimization of XCT scan parameters, ultimately enhancing segmentation accuracy

* Corresponding author at: imec-Vision Lab, Dept. of Physics, University of Antwerp, Universiteitsplein 1, Antwerpen, 2610, Belgium.
E-mail address: miroslav.yosifov@fh-wels.at (M. Yosifov).

https://doi.org/10.1016/j.measurement.2025.120168
Received 29 August 2025; Received in revised form 23 November 2025; Accepted 19 December 2025
Available online 22 December 2025

and the detection of small defects [19]. Moreover, X-ray simulation allows the estimation of uncertainties and provides the capability to control and isolate several types of physical effect such as focal spot blur effect, noise, virtual gain correction, modulation transfer function based unsharpness.

XCT has also become a key technology in industrial dimensional quality control over the past decade [20]. Its ability to assess multiple features simultaneously, without touching or modifying the object under investigation or facing sensor accessibility restrictions regarding small or hidden features, has led to its increasing adoption. Complex-shaped objects with tens, hundreds, or even thousands of dimensional measurement features can be inspected efficiently in a holistic way, offering significant advantages over traditional tactile or optical coordinate measurement systems [21]. The high information density provided by XCT renders this technology a crucial tool to address the challenges of contemporary manufacturing processes [22].

However, despite these benefits, XCT still faces major challenges when it comes to ensuring traceable dimensional measurements and to estimate measurement uncertainty. The complexity of the X-ray measurement process, combined with the simultaneous action of several physical effects makes it difficult to isolate and quantify their individual contributions to measurement deviations. Traditional experimental approaches for uncertainty estimation, such as the substitution [23] or multiple measurement methods [24,25], evaluate the system as a whole and thus cannot disentangle the influence of each effect within the measurement chain. As a result, the metrological understanding of how specific physical phenomena propagate through XCT and affect dimensional accuracy remains limited [26,27]. Simulation-based approaches offer a promising alternative to virtually investigate and experimentally explore these effects under controlled and repeatable conditions. By building a physics-based digital representation of the XCT process, it becomes possible to enable or disable individual physical effects and to assess their metrological significance in isolation. This digital strategy supports a deeper understanding of the mechanisms behind measurement deviations, promotes the development of simulation-based methods, and aligns with ongoing efforts in digital metrology and uncertainty evaluation using virtual measuring systems. In this context, this study aims to investigate the influence of selected physical effects on dimensional measurement deviations, namely virtual gain correction, focal spot blur, detector modulation transfer function, and Poisson–Gaussian noise in XCT. The proposed simulation framework enables isolating and quantifying each effect's individual contribution while maintaining consistency with real XCT data. By bridging simulation and experiment, this work advances uncertainty quantification in XCT metrology and provides insights to guide industrial users in optimizing scanning parameters and understanding which physical effects have the most significant metrological impact.

In this paper, we aim to address this knowledge gap by systematically investigating the influence of specific physical effects on measurement accuracy by employing XCT simulated. The key contributions of this work are threefold:

1. Isolate and quantify the individual contributions of different physical factors, such as virtual gain correction (VGC), Poisson-Gaussian (PG) noise, focal spot blur effect, and the modulation transfer function (MTF) on the detector, to measurement deviations;
2. Compare real XCT scans with simulated XCT data generated under various conditions, including different numbers of projections and with physical effects both enabled and disabled, to validate the simulation approach;
3. Provide actionable insights that can guide industrial practitioners in optimizing their XCT measurement processes by understanding which physical effects have the most significant impact on dimensional measurement accuracy.

Understanding these effects can contribute to developing strategies to reduce their impact and improve the overall accuracy of XCT measurements. The findings of this study may guide future efforts in improving measurement accuracy and developing more realistic simulation tools for XCT metrology.

2. Related work

Accurate dimensional measurements using XCT are highly dependent on understanding and controlling the various factors that influence measurement deviations (see Fig. 1). Several studies have explored different strategies to model these influencing factors and mitigate their impact on measurement accuracy. This section reviews recent advances in XCT metrology, focusing on estimating measurement uncertainty in XCT (Section 2.1), simulation-based studies for deviation analysis (Section 2.2), and relevant techniques for evaluating physical effects using X-ray simulations (Section 2.3).

2.1. Estimating measurement uncertainty in XCT

Measurement uncertainty is a fundamental concept in metrology, serving as an indicator regarding the quality of a measurement result, as it is defined as "a parameter associated with the result of a measurement that characterizes the dispersion of the values that could reasonably be attributed to the measurand" [29]. It quantifies the inherent doubt associated with measurement results, i.e., acting as an indicator of the quality and reliability of a measurement outcome. In the context of XCT, uncertainty estimation is challenging due to the multitude of influencing factors, ranging from system configurations (e.g., X-ray source and detector settings) to object properties (e.g., material composition and geometry), as also illustrated in Fig. 1. Traditional methods for estimating uncertainty, such as the substitution method [23], which determine measurement uncertainty by repeatedly measuring a geometry of a calibrated reference object, have been extensively used; however, they often lack the comprehensiveness required to address the complexity of XCT measurements.

Model-based methods, as outlined in the Guide to the Expression of Uncertainty in Measurement (GUM), provide a unified framework for uncertainty evaluation [30–32]. Since no analytical function is currently available to fully describe the CT measurement process, the law of propagation of uncertainty cannot be directly applied [30]. For this reason, numerical simulation has become a promising alternative. Following Supplement 1 to the GUM documentation [31], Monte Carlo trials can be used to evaluate how uncertainties in input quantities propagate through the measurement model. However, CT simulation requires significant computational resources, and commercially available software packages are not yet fully optimized for performing the large number of trials and considerations necessary to achieve statistically meaningful results [26,33]. Key challenges remain in identifying the most influential input quantities, isolating physical effects, assigning realistic uncertainty values to them, and determining the minimum number of simulations required to obtain reliable estimates [34–36]. Another approach, known as the substitution method [37], has its origin in ISO 15530-3 for tactile coordinate measuring machines and has been adapted for CT. This method is based on repeated measurements of calibrated workpieces similar to the actual workpieces of interest [38]. This technique requires that the calibrated reference and the test object be similar in geometry, size, and material, which is often difficult to realize in practice. As a result, many industrial implementations rely on calibrated reference artifacts or workpieces that do not fully represent the complexity of real parts [28]. This limits a general model of uncertainty estimation for actual measurement tasks. The process of evaluating measurement uncertainty can also be complemented by expert knowledge and metrologist judgment, particularly when choosing the most appropriate method for reporting uncertainty in CT measurement results. However, assessing the validity

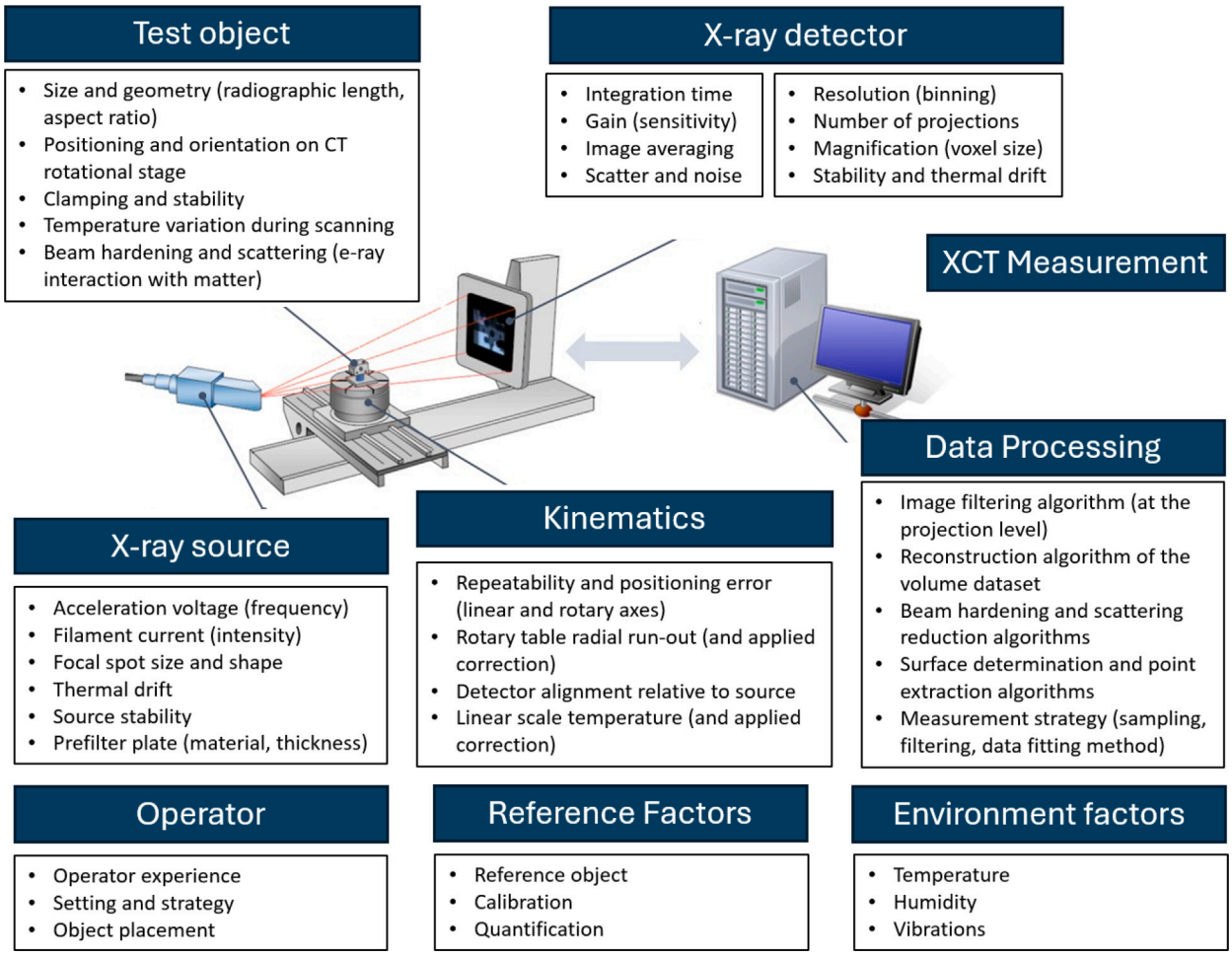

Fig. 1. Typical design of cone-beam XCT systems and factors influencing XCT dimensional measurements.
Source: Adapted from [28].

of corrections or assumptions is far from trivial and often requires considerable experience. A combination of different techniques can be adopted to develop more robust approaches to CT measurement uncertainty.

Several approaches have been proposed to estimate measurement uncertainty, emphasizing the need for comprehensive models that incorporate multiple error sources. For example, Dewulf et al. [27] presented a systematic framework for evaluating uncertainty in XCT measurements, thereby accounting for factors such as beam hardening, scatter effects, and surface determination errors. Similarly, Hiller et al. [39] introduced a parametric model that captures both geometric and radiometric uncertainties, providing a more holistic understanding of error propagation in XCT systems. Unlike earlier approaches [39–41] to XCT uncertainty estimation and analysis, which often relied on empirical error budgets or analytical models, our study employs X-ray simulations to isolate and examine individual error sources in a controlled virtual environment.

Recent developments have also highlighted the integration of machine learning techniques for uncertainty estimation. In large datasets of XCT measurements, respective models can predict uncertainty levels with greater accuracy compared to traditional analytical methods [42–44]. While being promising, the application of machine learning in metrology still faces challenges related to data quality, reproducibility, generalization and the interpretability [45]. In this context, physics-based XCT simulations, when sufficiently realistic, could support the training of such models by generating synthetic datasets with known reference values, as suggested in [42–44], helping to overcome the limited availability of labeled real-world data.

2.2. X-ray simulation for deviation analysis

X-ray simulation is a powerful tool for isolating and quantifying the influence of individual physical effects on measurement deviations. Using virtual environments, it is possible to control and manipulate specific parameters and effects such as VGC, PG noise, and focal spot blur to study their impact on measurement results. These simulations provide valuable insights that are difficult to obtain experimentally, enabling researchers to evaluate the sensitivity of the XCT system to different conditions.

Simulation-based studies have shown that the MTF plays an important role in the determination of the spatial resolution of XCT systems and hence the accuracy of dimensional measurements [46]. By simulating various focal spot sizes and detector configurations, researchers have been able to optimize the XCT system performance for specific applications [47]. Furthermore, advanced XCT simulation tools, such as XSimulation [48], ASTRA Toolbox [49], aRTist [50], or SimCT [51] and platforms to assess whether the digital twin sufficiently represents its real world counterpart such as CTSimU [52], have been employed to model and evaluate complex measurement scenarios, enhancing understanding of how physical effects propagate through the XCT imaging process and affect final measurements. In addition to system-specific factors, environmental conditions, such as temperature fluctuations and humidity variations, can introduce additional sources of uncertainty. Several studies have utilized XCT simulations to evaluate the impact of these factors, demonstrating that precise control of the scanning environment is crucial for maintaining measurement accuracy [53].

Table 1
Parameters for XCT imaging.

Parameters	Unit	Value	Parameters	Unit	Value
Acceleration voltage	kV	110	Source-object-distance	mm	120.43
Anode current	μA	155	Source-detector-distance	mm	1176.83
Integration time	ms	1s	Magnification	–	9.77
Detector pixels	–	2000x2000	Voxel size	μm	20.5
Number of projections	–	120 and 1000	Total cycle time	min	2 and 16

This line of research is particularly relevant for industries requiring high precision and metrological traceability, as it underscores the importance of developing robust XCT measurement protocols.

Despite all advantages, X-ray simulation also features limitations that can affect dimensional measurements. For example, often surface roughness or detector-specific artifacts are often not taken into account. While Poisson and Gaussian noise can be modeled, detector-based noise does not fully capture the statistical behavior and spatial correlations inherent in real detector responses. To address this limitation, a noise-sensitive image metric was applied in this study to measure the similarity and grey value profiles between simulated and real XCT data.

2.3. Evaluation of physical effects through X-ray simulation

Recent studies were focused on isolating and quantifying the impact of specific physical effects on XCT measurement accuracy. For instance, Villarraga-Gomez et al. [54] investigated the influence of X-ray scattering on dimensional measurements, proposing methods to correct for scatter-induced deviations. Similarly, Tan et al. [55] examined the effect of beam hardening on measurement accuracy and applied correction algorithms to mitigate its impact. The analysis of noise in XCT systems has also been a subject of recent research. Studies by Hiller et al. [56] and Reiter et al. [57] have explored various noise reduction techniques and their effectiveness in improving measurement accuracy, particularly for low-contrast features and thin-walled structures. Building upon these studies and focusing on the systematic analysis of individual physical effects, this work aims to provide a comprehensive understanding of how various factors contribute to measurement deviations in industrial XCT, ultimately leading to improved accuracy and reliability in dimensional metrology applications.

3. Materials and methods

This section describes the experimental and simulation procedures adopted in this study. The process starts with the acquisition of real XCT data (Section 3.1), followed by the generation of simulated XCT data under varying conditions (Section 3.2) and processing framework (Section 3.5). It concludes with a thorough analysis of the determined measurement deviations (Section 3.4).

3.1. Real XCT data acquisition

Real XCT data was acquired using a Nikon Metrology MCT225 system to validate the quality of simulated XCT data in terms of total uncertainty and image and volume similarity. Table 1 summarizes the main XCT imaging parameters used for the generated scans. To ensure optimal X-ray penetration and image contrast, the system was configured with an empirically determined acceleration voltage of 110 kV and anode current of 155 μ A. The integration time per projection was set to one second to balance signal-to-noise ratio and total scan time. The detector, a flat panel with 2000 × 2000 pixels and pixel size equal to 0.2 mm, provided high-definition imaging of the calibrated object with no binning applied.

To investigate the effect of projection count on deviation analysis, we initially generated CT data using five projection settings: 120, 250, 500, 750, and 1000. Since the deviation results for 500 and 750 projections were similar to those for 1000 projections, and 120 projections yielded results comparable to 250, this study presents findings from the 120 and 1000 projection datasets. The XCT images were reconstructed using the Feldkamp–Davis–Kress (FDK) algorithm [58], which has been widely adopted for cone-beam XCT imaging due to its computational efficiency and reconstruction accuracy. The scanning geometry was defined by a source-to-object distance of 120.43 mm and a source-to-detector distance of 1176.83 mm, yielding a magnification factor of 9.77. The voxel size was 20.5 μ m. The total scanning times for 120 and 1000 projections were approximately two minutes and 16 min, respectively. Fig. 2 shows the calibrated object along with the measured distances and cylinder holes analyzed in this study. The calibrated object was made of aluminum and contains 56 cylindrical holes. In this study, the diameters of 49 selected cylindrical holes (numbered 1 to 49), which were equally spaced in pairs during manufacturing, were evaluated, along with the distances between the centers of the corresponding cylinder pairs, as defined by the experimental design.

3.2. Simulation setup

XCT simulation was essential for this study, as it enables the isolation of various physical effects, which is not possible in real XCT scans. Simulated XCT data was generated using the software SimCT [51], incorporating detailed models of the XCT system components (source, detector, and rotary table) and the overall imaging process. The simulations were performed with distinct physical effects enabled – accounting for phenomena such as focal spot blur effect, the MTF on the detector, PG noise, and VGC – and another with the respective physical effects disabled, as such representing an ideal scenario. To mimic the XCT scanning conditions, the same XCT system and device characteristics were replicated in the simulations.

The CAD (Computer-Aided Design) model of the object, calibrated based on the dimensions obtained from a coordinate measuring machine (CMM), was converted into an STL (Standard Tessellation Language) file for use in the simulation. The voxel size in the simulated scans was set to 20.5 μ m to ensure consistency with the real XCT data. Similarly, the simulated projection data was reconstructed using the FDK algorithm. To further assess the impact of various parameters on measurement outcomes, simulations were carried out with different numbers of projections, i.e., 120 and 1000 projections, emulating different acquisition conditions. This approach allowed for the evaluation of image quality and measurement stability under varying sampling densities.

3.3. Physical effects modeled

Different types of physical effects were considered to understand their impact on measurement accuracy. These include PG noise, focal spot blur, the MTF on the detector, and VGC. Evaluating these effects helps to identify the key factors that contribute to uncertainty in the measurements. The selection of physical effects in this study was guided by their direct impact on dimensional measurement accuracy in industrial XCT applications. Focal spot blur was selected due to its direct impact on image sharpness and edge definition, which are relevant for accurate dimensional measurements. MTF was included as it characterizes the detector's ability to resolve spatial frequencies, affecting the overall system resolution. PG noise was chosen as it represents the fundamental quantum noise inherent in X-ray imaging,

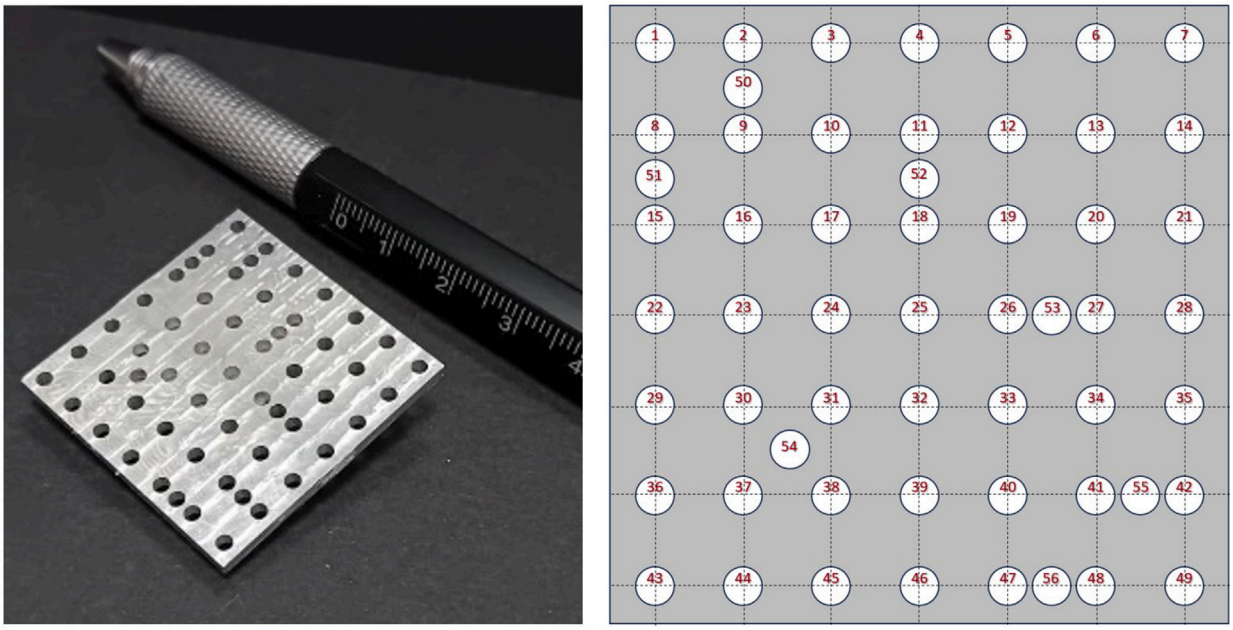

Fig. 2. Image of the calibrated object and visualization of its geometry. The diameter of each cylindrical hole is 2 mm, and the center-to-center distance between neighboring holes is 5 mm for holes numbered from 1 to 49.

while VGC was included as it is commonly employed in industrial XCT systems to compensate for detector non-uniformities but can introduce its own artifacts. These effects collectively represent the relevant physical influence quantities in typical industrial XCT systems and are thus critical for uncertainty evaluation and simulation-based measurement evaluation. The simulation framework was implemented using SimCT [51], enabling the independent activation of each physical effect to study its isolated contribution to measurement deviations.

Poisson-Gaussian noise distribution: The primary source of image noise is photon noise, which follows a Poisson distribution. This type of noise can be approximated by Gaussian-distributed random variables, with a variance that depends on the mean photon count [51]. When an integrating detector is employed, an additional Gaussian-distributed noise component, denoted as σ_G, is introduced. This noise originates from the dark current of the pixel's photo diodes and other general electronic noise. The noise model for the Nikon Metrology Flat Panel detector is represented by Eq. (1):

$$\sigma_{\mathrm{PG}} = \sqrt{\sigma_G^2 + \frac{I}{K}} \tag{1}$$

where I is the detected intensity measured in grey values, σ_G is the standard deviation, and K is a parameter that is experimentally determined based on various image acquisition parameters (e.g., detector gain, integration time, detected spectrum, etc.). Ultimately, Gaussian-distributed noise is added to each pixel's grey value using a random number generator, as shown in Eq. (1). This models the combination of Poisson and Gaussian distributed noise present in real X-ray images.

Focal Spot Blur modeled by a Gaussian Distribution: Focal spot blur refers to the blurring of the image due to the finite size of the focal spot. This effect can be modeled as a convolution of the initial image $I_0(x, y)$ with a Gaussian blur kernel $G(x, y)$ [51]:

$$I_{\mathrm{blur}}(x, y) = I_0(x, y) * G(x, y) \tag{2}$$

where $*$ denotes convolution, and the Gaussian blur kernel $G(x, y)$ is:

$$G(x, y) = \frac{1}{2\pi\sigma_b^2} \exp\left(-\frac{x^2 + y^2}{2\sigma_b^2}\right) \tag{3}$$

Here, σ_b is the standard deviation of the Gaussian blur and, x and y are coordinates in the plane perpendicular to the beam axis.

Modulation Transfer Function Based Unsharpness: The reduction in image sharpness can be modeled using MTF, such as those determined by the Slanted Edge Method proposed in ISO 12233 or its modifications. In addition to considering MTF-based unsharpness (the geometrical blur), the SimCT tool allows for the introduction of additional intensities to the virtually acquired images [51].

Virtual Gain Correction: VGC [59] adjusts the measured signal to account for non-uniformities or errors in the gain of the detector. The corrected intensity $I_{\mathrm{corrected}}(x, y)$ is given by:

$$I_{\mathrm{corrected}}(x, y) = \frac{I_{\mathrm{measured}}(x, y)}{GN(x, y)} \tag{4}$$

where $I_{\mathrm{measured}}(x, y)$ is the intensity measured at position (x, y), and $GN(x, y)$ is the gain correction factor at the same position.

The physical effects considered in this study – focal spot blur, detector MTF, PG noise, and virtual gain correction – propagate through the measurement chain and collectively influence the observed deviations. In the measurement chain, these effects primarily originate from the X-ray source and detector, affecting the radiograph images and, consequently, the reconstructed volume. At this stage, additional factors such as the number of projections and the performance of the reconstruction algorithm also play a role.

Specifically, focal spot blur reduces edge sharpness in the projections, directly impacting the reconstructed geometry of small features, such as cylinder diameters [60,61]. The detector's MTF further limits spatial resolution, smoothing fine details and interacting with focal spot blur to amplify edge uncertainties [61,62]. PG noise introduces stochastic variations in grey values, which propagate through reconstruction as local surface fluctuations; these fluctuations are more pronounced where edges are already blurred [63,64]. Imperfect virtual gain correction can leave residual systematic variations in grey values, which combine with stochastic noise and resolution limitations to produce small but measurable biases in reconstructed volumes [65,66]. In general, and from a theoretical standpoint, these effects are not independent. Their interactions can either amplify or partially compensate for one another, depending on the spatial region and the projection sampling density [61]. For instance, changing the focal spot size influences both the MTF and the virtual gain correction [60,65], while increased noise levels tend to worsen the impact of all other factors.

In certain scenarios, one physical effect may counterbalance the influence of another; however, when optimized scanning parameters are used – yielding acceptable image quality in terms of blur, sharpness, and noise – the individual physical effects become more stable and their relative contributions remain consistent [67].

3.4. Deviation and image similarity analysis

Measurement deviations were calculated by comparing the measurements performed on the data acquired by XCT (both real and simulated) to the reference values obtained from calibrated measurements results via CMM. This approach allows for quantification of the impact of different physical effects on measurement accuracy.

To evaluate the quality of the reconstructed 3D images, we employed the Structural Similarity Index (SSIM) [68] and the Peak Signal-to-Noise Ratio (PSNR) [69]. For segmentation analysis, the Jaccard Index and Dice Coefficient [70] were applied, as they are standard voxel similarity based metrics to quantify the overlap between predicted and reference segmented regions. SSIM and PSNR were selected because they allow us to capture both the numerical similarity (PSNR) and the perceptual similarity (SSIM), offering a more comprehensive evaluation of image quality between XCT data and simulated XCT data. PSNR provides a quantitative measure of pixel-wise fidelity, commonly used to assess how much noise or distortion is present in an image, while SSIM's incorporation of luminance, contrast, and structural information makes it more sensitive to spatial distortions that affect perceived visual quality. The following definitions and formulas are provided for the segmentation metrics.

Jaccard Index: The Jaccard Index measures the similarity between two sets by comparing the size of their intersection to the size of their union. For two binary images, A and B, the Jaccard Index $J(A, B)$ is defined as:

$$J(A, B) = \frac{|A \cap B|}{|A \cup B|} \tag{5}$$

where $|A \cap B|$ is the number of pixels where both images have non-zero values, and $|A \cup B|$ is the number of pixels where either image has a non-zero value.

Dice Coefficient: The Dice Coefficient [70] is another metric for comparing the similarity of two sets. It is particularly useful for comparing binary images. For two binary images, A and B, the Dice Coefficient $D(A, B)$ is given by:

$$D(A, B) = \frac{2|A \cap B|}{|A| + |B|} \tag{6}$$

where $|A \cap B|$ is the number of pixels where both images have non-zero values, and $|A|$ and $|B|$ are the number of non-zero pixels in images A and B, respectively.

3.5. Processing framework

A schematic representation of the complete processing pipeline, including the steps from XCT scanning to similarity analysis, is depicted in Fig. 3. The proposed processing pipeline begins with 3D metrology, where measurements such as the distance between points and the diameter of calibrated specimens were obtained using a CMM. This step is crucial because accurately determining these values allows us to compare them with the measurements obtained from XCT scans. These measurements were then additionally used to create a calibrated CAD model, which ensures that the digital representation reflects the calibrated dimensions of the object. Then, the CAD model was converted to the STL format to create a surface model of the calibrated object, which is widely used for XCT simulations.

Next, an XCT scan of the calibrated object was acquired, with a voxel size of 20.5 μm. The projection data was then reconstructed using the FDK algorithm. From the reconstructed data, diameters of the cylinder holes and distances between the cylinder centers were determined for analysis of measurement deviations. Three measurement repetitions were performed for each configuration to evaluate repeatability and to provide statistical descriptors for subsequent analysis. This number was chosen as a balance between experimental feasibility and the exploratory nature of the study. The analysis was performed using the software VGStudio MAX, with a custom macro (automation tool) created to streamline the measurement process across different XCT simulated configurations.

Simultaneously, numerical simulation was performed using the STL surface model, with the same voxel size of 20.5 μm. Two simulation conditions were considered: one with physical effects enabled, simulating real-world factors such as focal spot blur effect, detector MTF, PG noise, and VGC, and another with physical effects disabled, providing a controlled, ideal scenario. Additionally, with condition physical effects enabled, individual simulations were generated for each physical effect – MTF, PG noise, VGC, and focal spot blur – resulting in a total of six different simulations. The simulated XCT data was also reconstructed using the FDK algorithm, and measurements were determined from the simulated reconstructed data. Both real and simulated measurements undergo a comprehensive uncertainty analysis. The analysis assesses the total uncertainty and the physical effects (PE) inserted simulations uncertainty, the latter focusing on the impact of real-world physical factors introduced during the XCT scanning process.

After generating XCT scans and XCT simulations, a similarity analysis was conducted to compare the real and simulated data in terms of both image quality and uncertainty levels. This comparison ensures that the simulation accurately reflects the results of real XCT scans, given the conditions, supporting the validation of the simulated model in replicating physical phenomena and uncertainty sources typically observed in practice. Although these effects are simulated, they are designed to emulate physical influences present in actual scanning conditions.

4. Results and discussion

This section presents the evaluation of measurement uncertainty across different scenarios regarding deviations from calibration in cylinder diameters and center-to-center distances between cylinders. The analysis encompasses data from both XCT scans and numerical simulations, offering a comprehensive assessment of the physical effects that influence measurement accuracy, and the overall reliability of the simulations.

4.1. Deviations regarding internal diameters

X-ray simulations were performed using different STL models to achieve a deviation range similar to the range observed in real XCT data. For this purpose, two distinct STL models were initially employed: a nominal STL model extracted from the CAD model, and a "calibrated" STL model, which incorporates data obtained from reference measurements. The nominal STL model represents the design stage data of the object, in essence the expected dimensional measurement values prior to the manufacturing process. To create the "calibrated" STL model, measurement values obtained via a CMM were used to update the CAD model with real data prior to STL model extraction, in order to ensure a more accurate representation of the manufactured part. The similarity results for deviation were significantly higher when using a 'calibrated' STL model. Therefore, the "calibrated" STL has been chosen in order to improve the comparison with real scans. Subsequently, we generated the simulated data for the remainder of this study using the 'calibrated' STL model. Prior to dimensional evaluation, surface determination was performed in VGStudio MAX using a global ISO-50% threshold applied to the reconstructed grey-value volumes. After segmentation, the features of interest were evaluated through best-fit geometric fitting in the software's metrology module. For the hole diameters, circular fits were applied to the internal surfaces of the holes

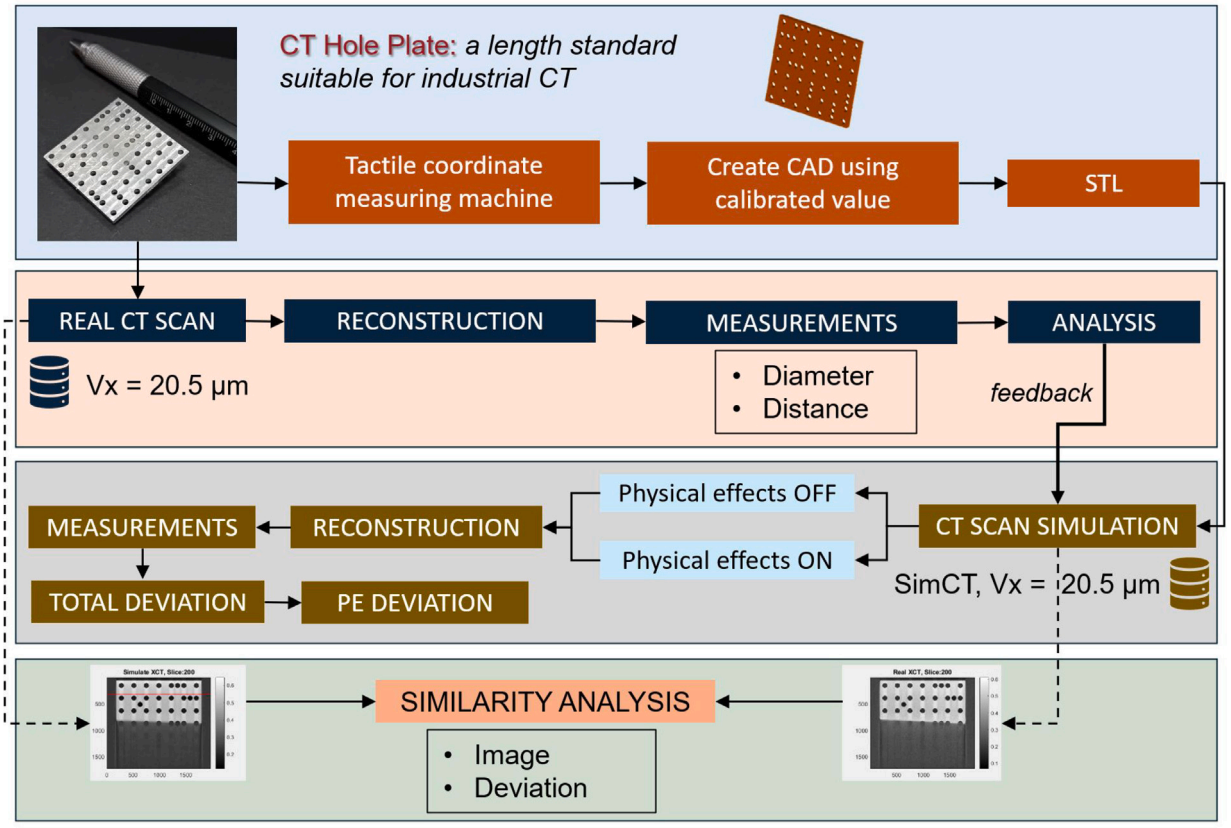

Fig. 3. Schematic representation of the proposed processing pipeline for comparing real and simulated XCT scans.

to obtain the effective measured values. Each dataset consisted of three repeated measurements, and statistical descriptors (mean, standard deviation, and range) were computed for every hole position to evaluate measurement repeatability and precision. The paired t-test confirms that the reduction in mean absolute error with 1000 projections is statistically significant ($p < 0.05$). The relatively narrow standard deviation observed across repetitions (below 0.005 mm) indicates good repeatability of the simulated measurement process.

The results of simulations were subsequently compared to a real XCT scan of the cylinder's internal diameter by evaluating both the simulated and real scans, and calculating the deviation in percentage from the calibrated value. The percentage of error values for the internal diameter were then normalized between 1 and −1 both for real and simulated scans using 120 and 1000 projections, indicating whether the determined diameter is higher or lower than the ground truth values. Fig. 4 presents an normalized error map illustrating comparisons between the XCT scan and the simulation by using 1000 projections. Each square in the error map represents a corresponding cylinder hole percentage of error values for diameter, numbered from 1 to 49, positioned identically to their layout shown in Fig. 2. These error maps effectively visualize the normalized percentage of error, indicating the extent to which each simulation deviates from the reference values derived from measurements via CMM.

Further analysis was conducted to evaluate how the number of projections in the simulations influence the accuracy of internal diameter measurements. Error maps were generated for simulations using 120 and 1000 projections, as illustrated in Fig. 5. Generally, an increase in the number of projections leads to a reduction in error, as indicated by the changes in the error map, and suggesting that higher projection counts improve accuracy in XCT data. However, simulations reveal that the error behavior remains consistent regardless of the number of projections, achieving a similar error range to that observed with the XCT data. In the simulations, the effect of the number of

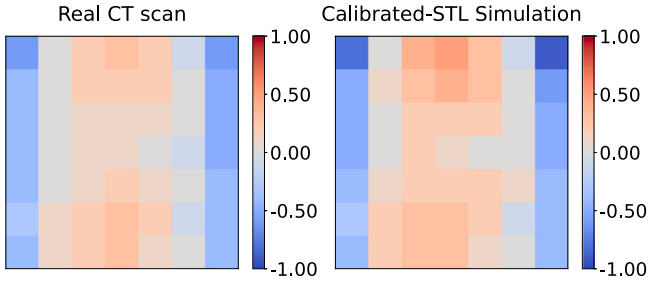

Fig. 4. Normalized error percentage in the internal diameter of the cylinders—deviation from CMM calibration (1000 projections used for the reconstructed volume). Each square in the error map corresponds to a cylinder hole (1–49) positioned as in Fig. 2 and shows the respective normalized percentage error in internal deviation.

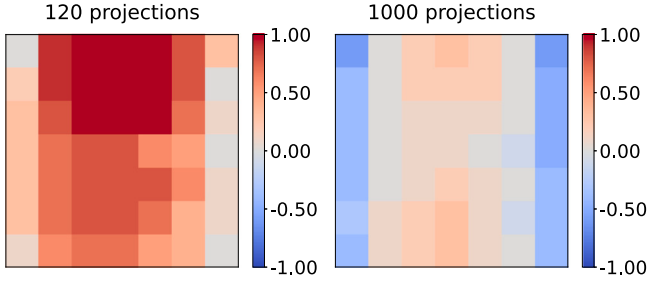

Fig. 5. Normalized error percentage in the internal diameter of the cylinder — deviation from CMM calibration, based on real XCT data. The error map shows how increasing the number of projections from 120 to 1000 reduces deviation from the calibration standard. Each square in the error map corresponds to a cylinder hole (1–49) positioned as in Fig. 2 and shows the respective normalized percentage error in internal diameter.

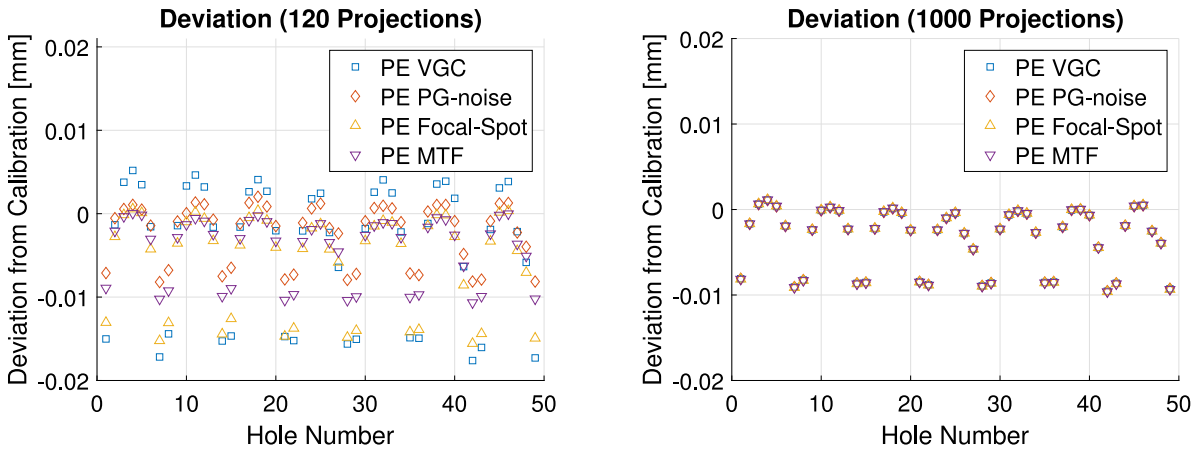

(a) Deviation with 120 projections

(b) Deviation with 1000 projections

Fig. 6. Deviation analysis for cylinder diameter in volumes created using by 120 (a) and 1000 projections (b). The plots show the deviations in cylinder diameter measurements due to different physical effects: VGC, PG noise, focal spot blur, and MTF.

projections on error behavior is minimal, whereas in the experimental XCT data, it shows a more noticeable impact. In particular, the simulated data for the 120-projection case do not fully replicate the characteristics of real CT data acquired with the same number of projections, mainly because the mounting system affects the quality of the final reconstructed image, especially in cases with a low number of projections. Nevertheless, the results remain largely comparable. Moreover, it is noteworthy that the errors in simulations generated with 120 projections are nearly equivalent to those in real CT data acquired with 1000 projections. This presents both an advantage and a limitation. On the advantageous side, for future experiments aiming to estimate the behavior of 1000-projection scans, simulations with fewer projections can provide a reasonable approximation. On the limitation side, improving the simulation to more accurately mimic the 120-projection case will require incorporating the effects of the mounting system or more advanced reconstruction algorithms. When comparing errors between XCT scans and simulations using 1000 projections, the results are nearly identical, indicating that the simulation accurately models the scanning conditions.

Statistical analysis of the error distributions reveals significant differences in the means and the standard deviations of the simulations with different numbers of projections ($p < 0.05$, paired t-test). The mean absolute error for measurements with 120 projections was 0.0112 mm (standard deviation 0.0043 mm), compared to 0.0068 mm (standard deviation 0.0025 mm) for measurements with 1000 projections. This represents a 39.3% reduction in mean absolute error when increasing the projection count, highlighting the quantitative benefit of higher sampling density. However, it also shows that the agreement between simulations and real scans worsens at lower projection numbers—a difference that may be influenced by the scanning strategy. The measurements were performed in continuous rotation mode. In contrast, the simulations were carried out in step-scan mode, as required by the implemented framework.

4.2. Physical effects analysis

This section presents the comparative results of the investigated physical effects in X-ray simulations. Fig. 6 shows a plot regarding the impact of these effects on the measurement accuracy of XCT simulations, comparing reconstructed volumes generated using 120 and 1000 projections in terms of inner diameters. Specifically, the analysis explores how the different physical effects, i.e., VGC, PG noise, focal spot blur effect from the X-ray source, and the MTF of the detector, affect the deviation of the measured cylinder hole diameters from the simulated data. In the simulations, individual physical effects were applied one at a time to isolate their specific influence on measurement deviations. For example, when a single effect such as MTF was enabled, all other scan conditions were not incorporated, i.e., there was no focal spot blur, no PG noise, and no VGC. The label PE ON refers to simulations in which all relevant physical effects were enabled simultaneously – including PG noise, focal spot blur, detector MTF, and VGC – thereby representing a realistic scanning scenario that closely approximates the experimental conditions. In particular, the VGC was implemented by dividing the measured intensity at each detector pixel by a pixel-specific gain correction factor, which was derived from an idealized detector response. This procedure accounts for detector non-uniformities and emulates the correction applied in real XCT systems, ensuring that the simulated data closely reflect the uniformity conditions achieved in experimental scans.

Fig. 6(a) provides an in-depth analysis of the deviation in cylinder hole diameter measurements when only 120 projections were used in the XCT simulation. It also highlights the impact of different physical effects on the measurement accuracy. The error range was notably higher in simulations generated with VGC (e.g., 0.023 mm). Moreover, the error range for PG noise, MTF, and focal spot blur effect simulations were respectively 0.016, 0.010 and 0.010 mm. These values are up to 56% lower than simulations generated with VGC (for a detailed view, see Table 2). The maximum absolute values (Max $|\Delta|$ [mm]) show that VGC and focal spot blur have an error of approximately 0.018 mm and 0.016 respectively, while MTF alone is around 0.010 mm, and PG noise contributes the smallest error, at about 0.008 mm. Table 2 additionally presents the minimum and maximum deviation values observed in the cylinder diameter measurements.

When comparing data between Figs. 6(a) and 6(b), it becomes clear that the deviations are more pronounced in 120 projections due to the lower number of projections, as it was expected. In Fig. 6(b), with 1000 projections, all physical effects exhibited similar behavior and resulted in lower deviation compared to the case with 120 projections.

The relationship between these physical effects and structural resolution, which is a critical factor in XCT metrology, warrants further examination. Structural resolution refers to the system's ability to resolve fine details and edges in the scanned object, which directly impacts dimensional measurement accuracy. The deviation results show that VGC and focal spot blur effect contribute most significantly to measurement deviations when using 120 projections. They also have the most significant impact on structural resolution. This is particularly evident in the edge regions of the cylinder holes, where the transition between material and air must be precisely captured for accurate diameter measurements.

Table 2
Error statistic for different physical effects modeled in XCT simulations, based on diameter deviation [mm].

Physical effect	Max $\|\Delta\|$ [mm]	Min [mm]	Max [mm]	Range [mm]
PE VGC	0.0176	−0.0176	0.0052	0.0228
PE Focal-Spot	0.0156	−0.0156	0.0006	0.0161
PE MTF	0.0107	−0.0107	0.0001	0.0107
PE PG-noise	0.0082	−0.0082	0.0020	0.0102

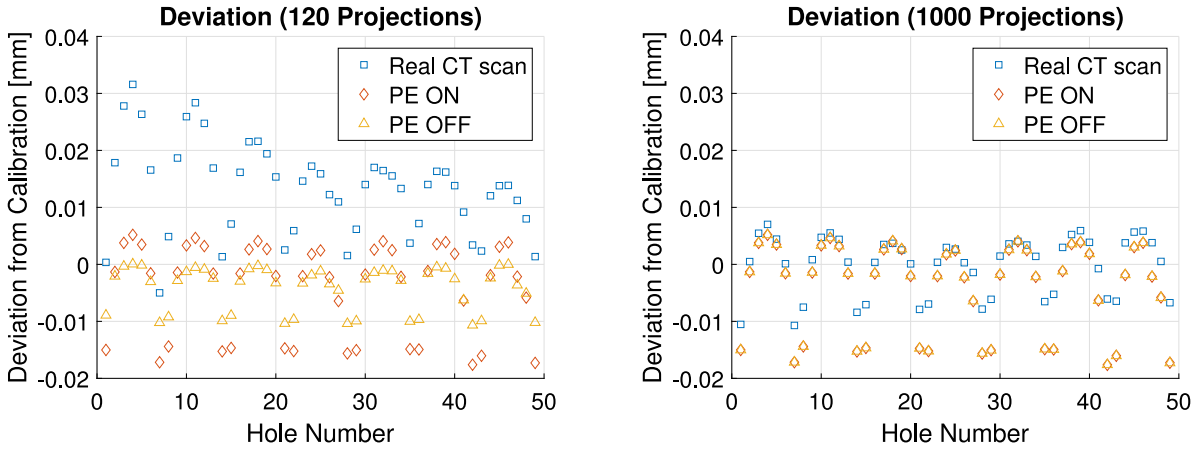

(a) Error with 120 Projections

(b) Error with 1000 Projections

Fig. 7. Cylinder diameter error between real XCT scans and simulation for different projection numbers.

4.3. Analysis of cylinder diameter deviation

Figs. 7 and 8 present a detailed comparison of cylinder diameter measurement errors between real XCT scans and simulations, considering both cases where the previously discussed physical effects (PE) were enabled (PE ON) and disabled (PE OFF). The figures also illustrate the influence of the number of projections and the role of physical effects on measurement accuracy. Fig. 7 shows the deviation when using 120 projections versus 1000 projections. With fewer projections (120), the real XCT scan data shows more variability and larger deviations from calibration. The XCT scan generated by 1000 projection case shows significantly reduced deviations, demonstrating the advantage of using more projections to achieve greater accuracy for real XCT data.

In the simulated data using 120 projections, the deviation range was smaller when physical effects were disabled in simulated XCT data. This indicates that introducing physical effects in the XCT simulation contributes to achieve a deviation range that more closely matches the real data. Upon comparing the error between the simulation and real XCT data generated by 1000 projections, the error difference was small, particularly the upper bound of the error, which was nearly identical between the real and simulated data. However, a noticeable difference of approximately 0.05 was observed in the lower bound, particularly for holes located at the left and right corners (e.g., holes 1, 7, 8, 14, 15, . . . , 49). This suggests that there is still room for improvement and warrants further investigation. Unexpectedly, in this case, the error results for simulations with and without the physical effect are the almost same. This suggests that, when using high projections, the inclusion of such physical effects may have negligible impact at least for the specific measurand evaluated in this study.

Fig. 8 further investigates these deviations after applying a correction that re-centers the data to normalize the error range between the maximum and minimum values observed in the real CT measurements. This normalization facilitates a clearer comparison of variability across datasets by removing global offset differences. It also enables a direct comparison of measurement deviations across different artificial effects and scan conditions, which may differ substantially in absolute magnitude. The deviation-corrected data for 120 projections shows that both PE ON and PE OFF results become closer to the real XCT data, though some differences remain on the left side, particularly between hole numbers 20 and 50. Although the recorded differences, the comparison of the ranges after applying the correction shows that PE ON leads to a better match with the real measurement range. Nevertheless, the results are very similar, considering that a low number of projections would inherently lead to greater variability. In the case of 1000 projections, the corrected data shows significantly lower deviations, and the real XCT scan data aligns closely with the simulations, both when physical effects were enabled and disabled.

Overall, these figures demonstrate that the role of physical effects in influencing the accuracy of XCT simulations when the images were generated using 120 projections. However, with an increasing number of projections, the errors for simulations with and without PE converge, suggesting that the physical effect becomes less significant. The final key observation is that, with 1000 projections and error correction, the deviation between simulated and real XCT measurements converge to nearly identical values.

4.4. Analysis of center-to-center distance deviations

This section presents an analysis of the deviations in center-to-center distance measurements between the cylinder holes in the calibrated object (see Fig. 9), comparing real with simulated XCT data. This comparison evaluates how closely XCT simulation aligns with real-world measurements and assesses the impact of the number of projections (120 vs. 1000) on measurement accuracy. The center-to-center distances analysis were evaluated entirely in 3D by fitting cylinders to the hole surfaces and calculating the distances between the corresponding cylinder axes. This approach avoids any dependence on specific cross-sectional planes and ensures 3D consistency of the measured features.

Fig. 9 presents boxplots illustrating the deviations from calibration for center-to-center distance measurements using 120 and 1000 projections in both real XCT scan and simulated data. Each boxplot corresponds to a different nominal center-to-center distance measurements between cylinder holes, ranging from 5 mm to 30 mm. The central

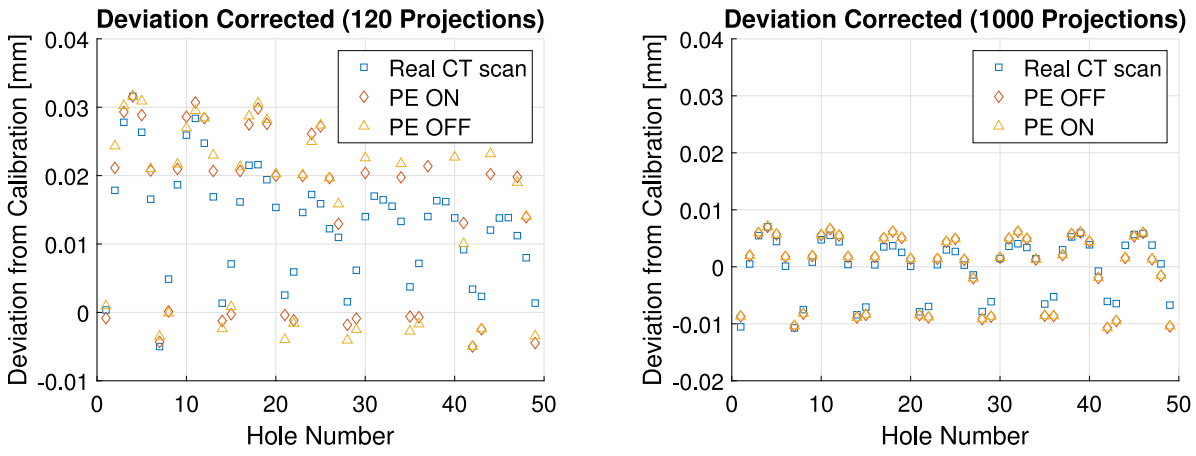

(a) Error with 120 Projections

(b) Error with 1000 Projections

Fig. 8. Corrected cylinder diameter error between real XCT scans and X-ray simulation for different projection numbers.

line in each boxplot represents the median deviation, while the box denotes the interquartile range, and red plus signs indicate outliers. These visualizations provide insight into the accuracy and consistency of the measurements across different projection counts.

Fig. 9 reveals that Figs. 9(a) and 9(b) display deviations from real XCT scan data, whereas Figs. 9(c) and 9(d) show the corresponding deviations from the simulated data with physical effects enabled. Both real and simulated data exhibit a clear trend: increasing the number of projections (from 120 to 1000) reduces the spread of deviations, indicating improved measurement accuracy. However, a notable difference emerges in simulated data, which demonstrates a narrower deviation range, particularly in the 120-projection case.

A radiography from real XCT scan, its corresponding grey value map, and the grey value profile along the indicated line are presented in Fig. 10. We observed that image artifacts were particularly noticeable in the radiographs from both 120 and 1000 projections case, especially in the half portion of the images (see Fig. 10). These artifacts appear consistently across all projection images in both the 120- and 1000-projection cases. Based on the characteristic shape (see Fig. 10) and their consistent appearance across all projections, we found that the artifacts are caused by the specimen holder and its supporting system. However, this holder was not included in the simulations, which explains the differences observed between the simulated and real XCT data. Additionally, the results indicate a correlation between these artifacts and higher deviations observed in the region of cylinder holes indexed from 1 to 25 (see also Figs. 7 and 9(a)) for the 120-projection case. A further note is that this artifact is not visible in the reconstructed volume obtained from both the 120- and 1000-projection datasets; however, it still appears to affect the deviation measurements in 120 projection case. The results indicate that the influence of this artifact is minimal in the 1000-projection case, while it is noticeably higher in the 120-projection case. This issue could potentially be mitigated by employing an improved reconstruction algorithm. In future work, the workflow could also be extended to include simulation of the specimen holder, allowing for more accurate reproduction and analysis of these artifacts.

Remarkably, when using 1000 projections, the deviation ranges in real and simulated data become more similar, suggesting that simulations generated with high projections can closely mimic real XCT scan results. Furthermore, the deviations obtained from 120 projections in the simulated data closely resemble those from 1000 projections in the real data. It is important to clarify that the difference in scanning modes – step mode for simulations versus continuous mode for real scans – may significantly contribute to the observed discrepancies, particularly given the lower number of projections in the simulated data. This difference could affect the accuracy of the simulated results as previously considered artifacts, such as those related to the mounting system. To improve the comparison, simulations of continuous scans are needed to better align with the real data acquisition protocol when using the low number of the projections. This observation implies that even with a reduced number of simulated projections, it is still possible to estimate deviations in high-quality XCT measurements.

These findings highlight the effectiveness of the simulation based approach for replicating real-world measurements especially for the case 1000 projection. Ideally, simulated data should align with real XCT scan results, even when generated with a low number of projections, reinforcing the validity of the simulation methodology and its potential for accurate measurement analysis in various applications.

4.5. XCT data visualization and image similarity analysis

Visualization and image similarity analysis are key tools to validate simulated deviations against real-world experiments. Fig. 11 and Table 3 demonstrate the influence of the number of projections on the quality and similarity of XCT simulations compared to real XCT images. In Fig. 11, the left panel shows image slices of simulated data generated with 120 projections, compared with real CT data acquired using 1000 projections, while the right panel presents the corresponding slices from volumes reconstructed with 1000 projections for both the simulation and the real CT data. Each panel includes XCT simulation images (top row), real XCT images (middle row), and corresponding grey value profiles along a marked line (bottom row). For 120 projections, the simulation exhibits noticeable discrepancies compared to real XCT data with visible differences in the grey value profiles, especially around regions representing holes. In contrast, using 1000 projections, the XCT simulation closely matches the real XCT, as evidenced by the nearly overlapping grey value profiles, indicating a high degree of similarity. Table 3 provides quantitative metrics for these comparisons, showing a significant improvement in SSIM, PSNR, and segmentation accuracy (Jaccard and Dice coefficients) as the number of projections increases from 120 to 1000. Normalization was applied to compute SSIM using MATLAB's `ssim` function, which requires input values in the range $[0, 1]$. The `mat2gray` function was used to scale the images accordingly. The maximum and minimum grey values of the real data were similar to those of the simulated data, ensuring that the normalization does not alter the underlying image characteristics. Therefore, potential differences due to outliers do not affect the results. Specifically, SSIM rises from 0.8669 to 0.9645, PSNR from 24.1 to 34.72, and both Jaccard and Dice coefficients improve from 0.94 and 0.97 to 0.98 and 0.99, respectively. These results underline the importance of a higher

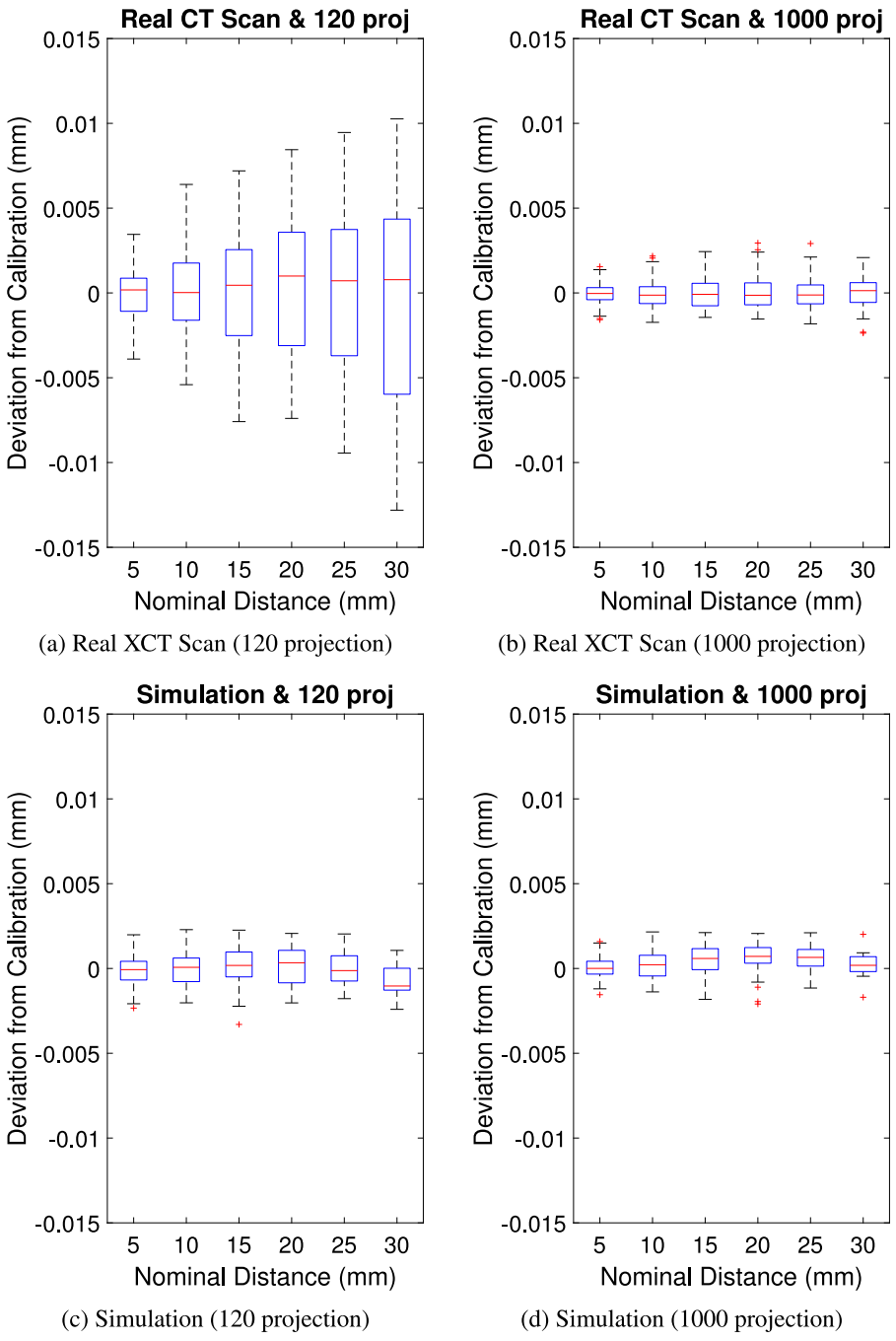

(a) Real XCT Scan (120 projection)

(b) Real XCT Scan (1000 projection)

(c) Simulation (120 projection)

(d) Simulation (1000 projection)

Fig. 9. Deviation from calibration in center-to-center cylinder distance measurement on XCT and simulated data.

number of projections in achieving more accurate and higher-quality XCT simulations that better replicate real XCT scans. A critical point to note is that when comparing the 3D volume similarity between simulations and XCT data for 120 projections, using the Dice coefficient, the similarity index increases from 0.97 to 0.99. This suggests that the impact of the number of projections becomes significantly less noticeable in the segmented images. Further evidence of this was seen when measuring the distance between cylinders of a volumetric dataset reconstructed from 120 projections, even though the image similarity shows a 2% difference in the Dice coefficient metric, we can still achieve results that are almost identical to those from a real XCT scan generated with 1000 projections.

Fig. 12 visually compares the impact of different type of physical effects (PE) on the intensity distribution of simulated XCT images. The top row showcases axial slices processed with different PE methods: focal spot blur effect, noise, MTF, and VGC. These images highlight the noticeable differences in image quality resulting from each PE correction. Visual differentiation of the effects of Focal-Spot, noise, MTF, and VGC corrections on XCT images (Fig. 11, top row) is challenging. To quantitatively assess impact of these variations, the bottom plot presents intensity line profiles extracted along the red line marked in the images, spanning positions 1000 to 1100. This analysis reveals distinct differences in intensity, contrast, and edge response across the different PE, offering a detailed insight into their effects on the final image quality. An inset further zooms into the 1010-1030 range to emphasize local intensity variations.

Results from Fig. 12 and the deviation analysis suggest that MTF is the primary factor contributing to image unsharpness, though its impact on uncertainty is getting smaller. When correlating these findings with deviation analysis, it becomes evident that VGC and focal spot blur

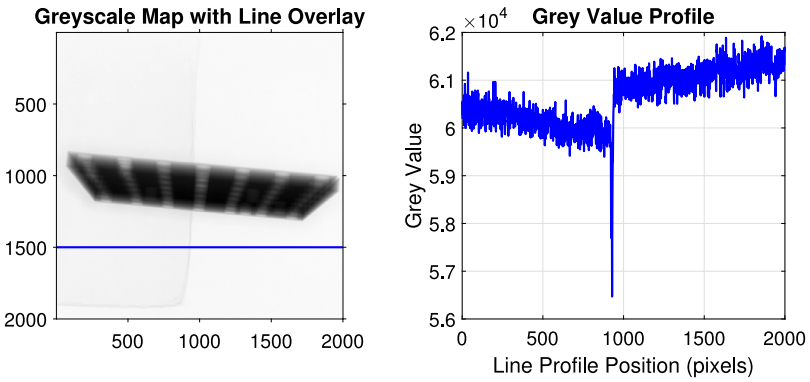

Fig. 10. Visualization of a radiograph slice with a profile analysis. Grayscale image of the radiograph with a superimposed horizontal line (blue) placed 500 voxels below the vertical center, indicating the location used for intensity profiling. (Right) Corresponding grey value profile plotted along the marked line, illustrating the variation in pixel intensity across the horizontal axis of the image.

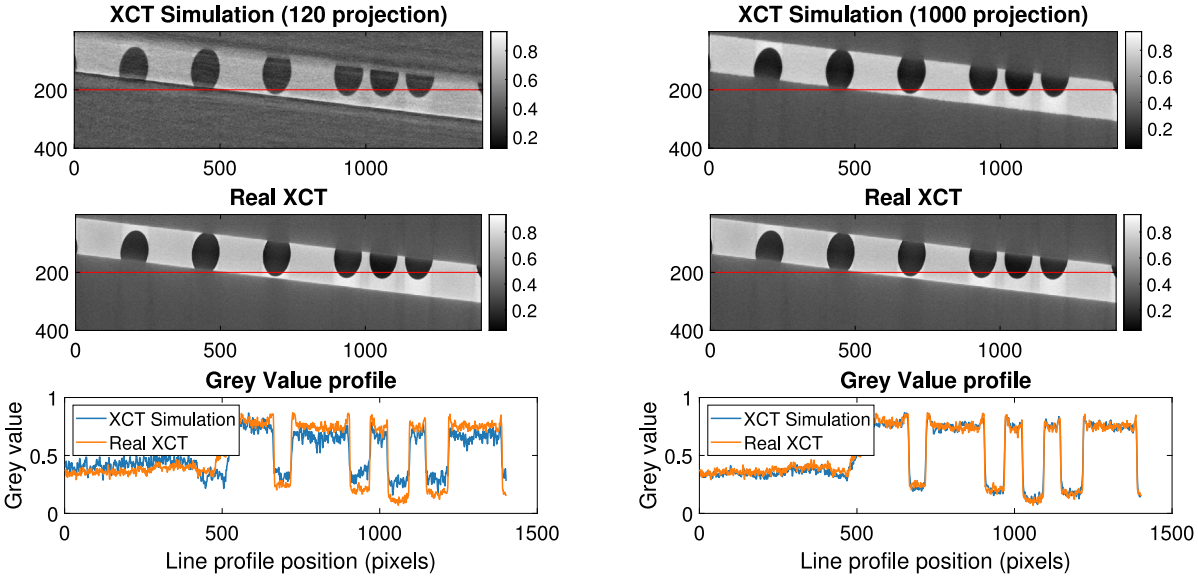

(a) (b)

Fig. 11. Comparison of XCT simulations using 120 and 1000 projections against real XCT images. The top and middle rows show XCT simulations and real XCT images, respectively, while the bottom row displays grey value profiles along the marked red line. **Note:** The grey values were normalized to the range [0, 1].

Table 3
Image similarity metrics: comparing simulation results with XCT data from 1000 projections in 3D volume.

XCT simulation	SSIM	PSNR	Jaccard index	Dice coefficient
120 projections	0.8669	24.10	0.94	0.97
1000 projections	0.9645	34.72	0.98	0.99

factors play a more significant role in deviation errors. Interestingly, noise, which was initially considered a primary source of error, does not appear to have a substantial effect. An important observation was that at the image edges, both the focal spot blur effect and VGC exhibit similar sharpness behavior, with only slight differences (see Fig. 12). However, this seemingly minor difference in sharpness has a considerable impact on deviation, underscoring the high sensitivity of the measurements to variations in sharpness.

Additionally, a ground truth reference was created for comparison. Fig. 13 shows a comparison between the simulated dataset (PE ON) and the real CT scan in terms of intensity distribution. The top row presents the corresponding XCT images for both cases, while the bottom plot illustrates the intensity line profiles extracted along the red-marked region in the images (positions 1000–1100). The close agreement between the two profiles indicates that the simulation incorporating all physical effects (PE ON) successfully reproduces the overall intensity behavior observed in the real CT data.

4.6. Comparative discussion with related research

This section compares the simulation-based findings with existing literature on XCT dimensional metrology and image similarity, focusing on the effects of projection number and the use of calibrated hole-plate standards.

4.6.1. Effect of projection number on XCT and dimensional accuracy

The number of projections in a CT scan is a key factor influencing both image quality and dimensional measurement accuracy. Several studies have investigated this effect systematically. In the recent study,

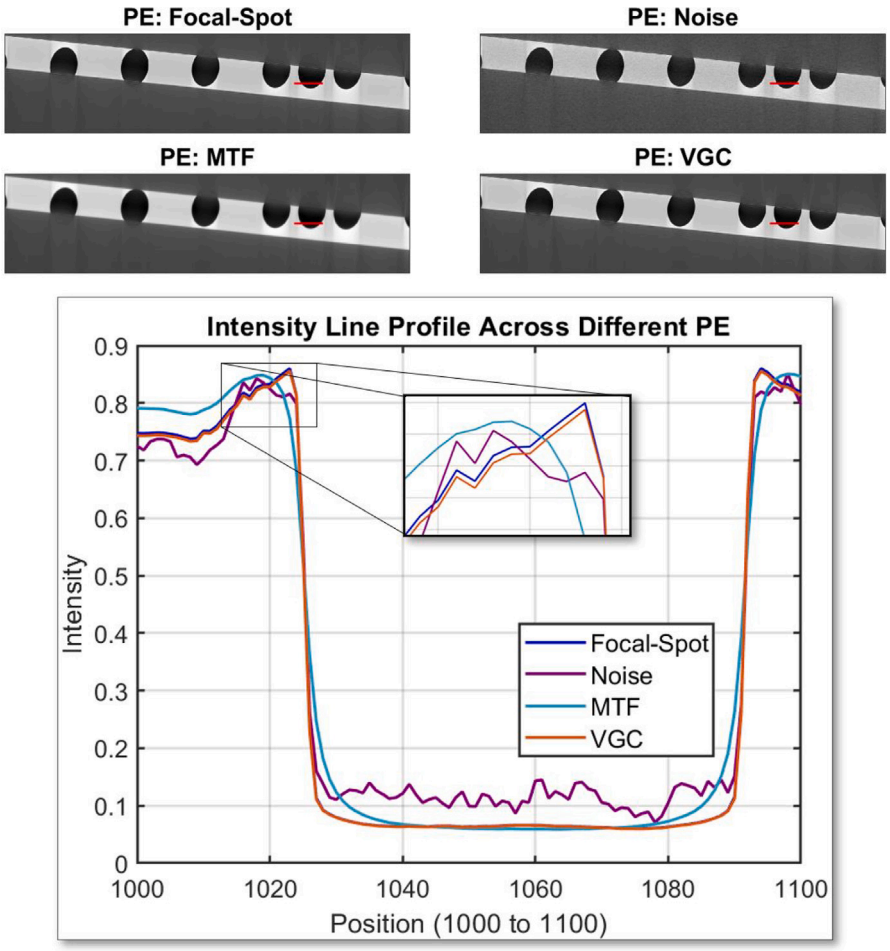

Fig. 12. Comparison of different physical effects (PE) on intensity distribution. The top row displays XCT images processed with various PE methods: Focal-Spot, Noise, MTF, and VGC. The bottom plot shows intensity line profiles along the region marked in red in the images, covering positions 1000 to 1100. The variations in contrast and edge response across different PE methods are highlighted. An inset zooms into the 1010-1030 range for a clearer view of local intensity differences.

Villarraga-Gómez et al. [71] investigated how the number of projections (N_p) affects dimensional accuracy in X-ray computed tomography. They reported that when N_p falls below approximately 600, dimensional measurement errors – particularly form deviations – increase rapidly, reaching values well above 100 μ m when compared to tactile CMM reference measurements. They also evaluated image-quality metrics such as PSNR, MSSIM, and RMSE, showing that reconstruction quality improves monotonically with N_p up to about 1000 projections, beyond which diminishing returns are observed. Our simulation-based results show that, in the case of 120 projections, the maximum absolute deviation is approximately 30 μ m for real CT, while simulations yielded approximately 20 μ m. For instance, increasing the number of projections from 120 to 1000 raises SSIM from ~ 0.867 to ~ 0.965 and PSNR from ~ 24.1 dB to ~ 34.7 dB, while segmentation overlap metrics (Jaccard and Dice coefficients) improve from 0.94/0.97 to 0.98/0.99.

Additional studies provide complementary context. Sun et al. [72] showed that aggressive undersampling combined with total-variation reconstruction can yield acceptable volumetric reconstructions while dramatically reducing scan time (from ~ 52 minutes to ~ 1 minute), although improvements in SSIM and PSNR are more modest due to real-world noise and detector imperfections. Orgeldinger et al. [73] experimentally investigated the effects of projection number and scan mode on dimensional measurement accuracy and observed that reduced projections can significantly influence results, especially under continuous scanning or depending on object positioning. In the present study, the standard FDK algorithm was applied for reconstruction; using an advanced reconstruction algorithm can improve image quality for the 120-projection case in both real and simulated data, allowing image similarity to approach that of the 1000-projection case. Importantly, the main difference observed here is that our simulation results with 120 projections closely match the deviations obtained with 1000 projections, both in simulated and real data.

Overall, these comparisons indicate that while our quantitative gains in image similarity and segmentation overlap are larger than those reported in previous experimental studies, the qualitative behavior is consistent: increasing the number of projections improves both image fidelity and dimensional accuracy.

4.6.2. *Comparison using calibrated hole-plate standards*

Compared with the PTB hole-plate used in previous studies, the calibrated object examined in our work features a different geometry and measurement design. While many earlier investigations – such as those by Binder et al. [74], Villarraga-Gómez et al. [75,76], and Rossides et al. [77] – utilized PTB steel or aluminum hole plates containing approximately 28 precision-machined holes with diameters typically around 0.5–1 mm and center-to-center spacings tailored for metrological traceability, our study employs a larger aluminum artifact consisting of 56 cylindrical holes. Of these, 49 holes (numbered 1 to 49) were selected for analysis; they are arranged in equally spaced pairs, each with a diameter of 2 mm and a fixed center-to-center distance of 5 mm. Additionally, another key difference is that these previous studies did not apply any image similarity metrics and focused primarily on total dimensional deviations.

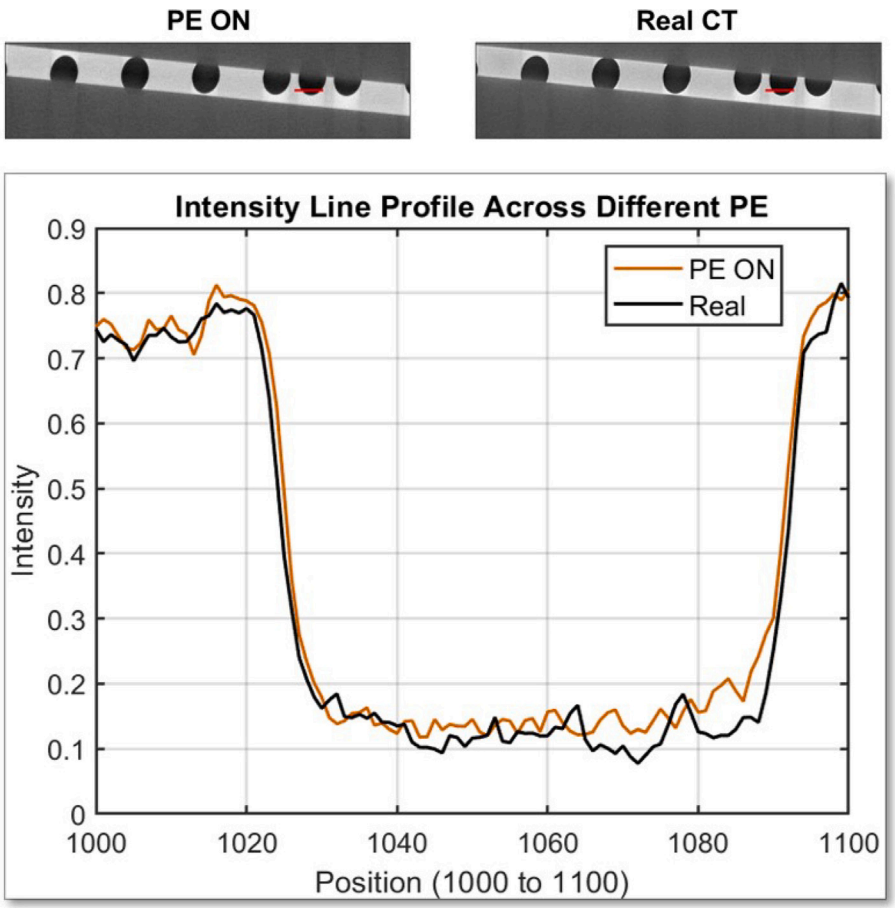

Fig. 13. Comparison between the simulated dataset (PE ON) and the real CT scan based on intensity distribution. The top row shows the corresponding XCT images: PE ON and Real CT. The bottom plot shows intensity line profiles along the region marked in red in the images, covering positions 1000 to 1100.

Other comparable studies on XCT measurements using hole-plate standards have been reported in the literature related to CT for dimensional metrology. Bartscher et al. [67] introduced the use of hole plates as reference standards for testing length measurement errors in XCT, incorporating the material influence on the results and demonstrating the applicability of this type of CT artifact for measurement accuracy analysis. In a subsequent study, Bartscher et al. [78] performed additional experiments using hole plate artifacts and corresponding measurement analyses to assess length-measurement errors and to evaluate the behavior of uni- and bidirectional measurands. Building on this design concept. Some time later, Sbettega [79] investigated measurement accuracy enhancement of industrial XCT systems through the metrological characterization of error sources using hole-plate artifacts, focusing on the impact of scanning orientations and the influence of material on the performance verification of industrial CT systems. The present study differs from these works by focusing on the isolation of individual physical effects (VGC, focal spot blur, MTF, and PG noise) rather than on overall system performance or artifact design. This approach enables the separate quantification of each effect's contribution to the total measurement deviation, providing a more detailed understanding of how these phenomena influence dimensional accuracy in industrial XCT metrology.

4.7. Limitations and practical implications

The results demonstrate a good level of agreement between real and simulated XCT data, both in terms of geometric deviations and image similarity, but some limitations must be acknowledged. In the present simulations, artifacts related to the mounting system and small geometric misalignments during scanning were not modeled. These factors can influence grey-value distributions and the geometry of measured features. The simulations were carried out using a step-scan acquisition mode, whereas the real XCT scans were performed in continuous rotation. These differences explain some discrepancies observed at lower projection counts. Other environmental influence quantities, such as temperature variations, detector lag, and mechanical stability, were not included and could contribute to the overall measurement uncertainty in real setups.

A further limitation is the restricted generalizability of the results to complex geometries, multi-material objects, and varying voxel resolutions. This limitation is not unique to our study; generalizability is a common challenge in uncertainty evaluations, as changes in specimen geometry, material composition, or imaging resolution can all influence the resulting measurement uncertainty in experimental XCT procedures [25,80,81]. Extending the methodology to handle multi-material and complex-shaped specimens, as well as varying voxel resolutions, is planned for future work.

The findings may have practical implications for industrial XCT metrology. The quantitative analysis confirms that virtual gain correction and focal spot blur are the dominant contributors to dimensional deviations, indicating that these effects should be prioritized when optimizing system calibration or estimating measurement uncertainty. The results also show that reduced-projection acquisitions can still provide reliable deviation estimates when appropriate calibration procedures are applied, offering opportunities to shorten scanning time without compromising measurement accuracy. The proposed simulation-based framework provides useful guidance for practitioners seeking to balance scan duration and accuracy in dimensional XCT measurements.

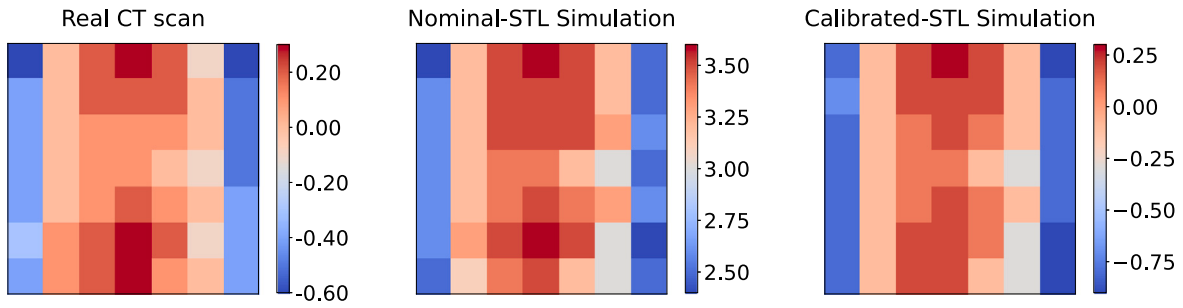

Fig. A.1. Error percentage in the internal diameter of the cylinders—deviation from CMM calibration (1000 projections used for the reconstructed volume). Each square in the error map corresponds to a cylinder hole (1–49) positioned as in Fig. 2 and shows the respective normalized percentage error in internal deviation.

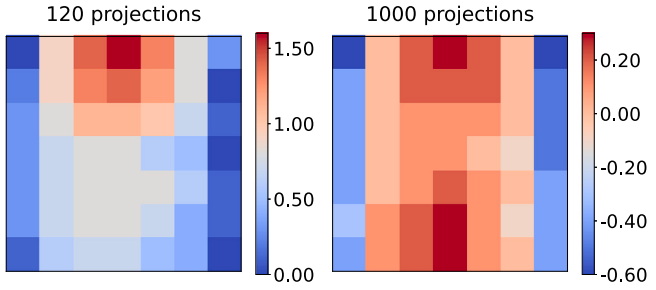

Fig. A.2. Error percentage in the internal diameter of the cylinder — deviation from CMM calibration, based on real XCT data. The error map shows how increasing the number of projections from 120 to 1000 reduces deviation from the calibration standard. Each square in the error map corresponds to a cylinder hole (1–49) positioned as in Fig. 2 and shows the respective normalized percentage error in internal diameter.

The quantitative evaluation in this work was based on three repeated measurements for each configuration. Although this repetition number limits a full statistical uncertainty characterization, it provides sufficient information to assess repeatability and to perform significance testing for the investigated effects. A complete uncertainty budget following the ISO GUM framework [30–32] was not included, since the study was designed to isolate and quantify the relative influence of individual physical effects rather than to provide an expanded uncertainty statement. Future work will expand this framework toward a full uncertainty evaluation to further support the measurement traceability and simulation-based dimensional XCT measurements.

5. Conclusion

This study has demonstrated the importance of understanding and quantifying individual physical effects in XCT imaging for improving measurement accuracy in XCT metrology. The insights gained from this research can thus contribute to the development of more accurate XCT systems, improved simulation tools, and more reliable quality control processes in manufacturing industries. Furthermore, as simulation models become increasingly representative of real-world measurements, they hold strong potential for supporting a prior uncertainty estimation—an aspect highlighted in the introduction and essential for advancing XCT-based dimensional metrology.

More specifically, it has provided insights and proved evidences regarding individual sources of measurement deviations associated with physical effects in XCT imaging. By comparing XCT data with simulated XCT data generated under various conditions, we have quantified the impact of different physical effects on measurement accuracy in industrial XCT metrology. The main findings can be summarized as follows:

- The consideration of physical effects in simulations is crucial for accurately representing real XCT behavior and for reproducing realistic uncertainty and deviation patterns.
- In this study, the number of projections was found to significantly influence measurement accuracy at a resolution of 20.5 µm in real XCT data. However, in simulated data, even with just 120 projections, the deviations remained relatively comparable to those observed with 1000 projections, suggesting that low projection counts may still provide acceptable accuracy for estimating deviations.
- Different physical effects contribute to measurement deviations at a varying degree. VGC and the focal spot blur effect were found to have the most significant impact on measurement accuracy (up to 0.018 mm deviation), while PG noise had a relatively small effect (approximately 0.008 mm). This hierarchy of influence provides practical guidance for XCT practitioners on which factors to prioritize when optimizing system performance.
- The image similarity index, along with the visual representation of XCT and simulated data, demonstrates that the performed simulations are comparable to real XCT data when generated using 1000 projections. This further validates both the error values observed in our analysis and the suitability of the simulation approach for studying physical effects in XCT imaging.
- Edge image analysis shows that while MTF contributes to image unsharpness, deviation errors are more strongly influenced by focal spot blur and VGC, with even minor sharpness differences at image edges having a significant impact on measurement sensitivity.

The methodology developed in this study provides a novel approach for understanding individual physical effects in XCT imaging. This approach can be extended to other XCT systems and measurement scenarios, potentially leading to more accurate and reliable XCT metrology across various industrial applications. For practitioners in the field of industrial XCT metrology, main findings suggest the following practical recommendations:

1. When optimizing XCT scanning parameters for dimensional measurements, prioritize factors that minimize VGC artifacts and account for focal spot blur effect, as these have the largest impact on measurement accuracy.
2. When time constraints limit the number of projections that can be acquired, ensure that careful calibration of the system and reference models are employed to compensate for the reduced sampling density.
3. For critical dimensional measurements, especially of internal features, consider the potential impact of edge effects and structural resolution limitations on measurement accuracy, and select scanning parameters accordingly.
4. When developing uncertainty budgets for XCT measurements, allocate greater weight to components related to VGC and focal spot, as these contribute more significantly to overall measurement deviations.

The findings of this study contribute to a better understanding of how individual physical effects influence dimensional measurement deviations in XCT. The results confirm that virtual gain correction and focal spot blur are the most relevant sources of deviation, followed by MTF and Poisson–Gaussian noise. The use of a physics-based simulation approach allowed the quantitative assessment of these effects under controlled conditions, showing that simulations can reproduce the behavior of real XCT data with high similarity. Beyond the presented research, the results indicate that simulation can be used as a practical tool to support CT measurement process and to complement experimental validation in dimensional XCT metrology. This approach can help reduce the need for extensive repeated measurements and enable more efficient planning of XCT inspections in industrial environments.

Future work will focus on several areas, including developing methods for estimating measurement uncertainty, or exploring machine learning techniques with XCT simulations. Potentially machine learning could accelerate the determination of measurement deviations and optimize scanning parameters through investigations of the impact of environmental factors and material properties on measurement deviations in industrial XCT. One possible solution is to use supervised learning approaches, where machine learning models are trained to predict deviation bias based on validated simulated XCT scans (radiographs or reconstructed volume), image quality metrics, and the number of projections. The output will be the estimation of measurement deviations and uncertainty. Then, the trained models would predict deviation trends and provide real-time recommendations for optimizing scanning parameters to minimize measurement uncertainty. Additionally, future research will extend the framework to more complex geometries, multi-material objects, and varying voxel resolutions, which are increasingly relevant in advanced manufacturing contexts. Ultimately, the combination of X-ray simulation and machine learning may further improve uncertainty estimation and support the transition toward fully automated, digitally assisted XCT metrology.

CRediT authorship contribution statement

Miroslav Yosifov: Writing – review & editing, Writing – original draft, Visualization, Validation, Software, Resources, Methodology, Investigation, Formal analysis, Data curation, Conceptualization. **Thiago Linhares Fernandes:** Writing – review & editing, Validation, Methodology, Investigation, Formal analysis, Data curation, Conceptualization. **Filippo Zanini:** Writing – review & editing, Validation, Supervision, Methodology. **Simone Carmignato:** Writing – review & editing, Supervision, Conceptualization. **Jan De Beenhouwer:** Writing – review & editing, Supervision, Conceptualization. **Jan Sijbers:** Writing – review & editing, Supervision, Conceptualization. **Johann Kastner:** Writing – review & editing, Supervision, Funding acquisition. **Christoph Heinzl:** Writing – review & editing, Visualization, Supervision, Funding acquisition, Conceptualization.

Declaration of Generative AI and AI-assisted technologies in the writing process

During the preparation of this work, the author(s) used ChatGPT for language editing purposes only. After using this tool, the author(s) thoroughly reviewed and edited the content as needed and take full responsibility for all aspects of the published article.

Declaration of competing interest

The authors declare that they have no known competing financial interests or personal relationships that could have appeared to influence the work reported in this paper.

Acknowledgments

We acknowledge primary financial support from the project sustaiNDT (grant no. 909801), funded within the framework "Production & Materials" of the Austrian Research Promotion Agency (FFG). This research was co-financed by the European Union H2020-MSCA-ITN- 2020 under grant agreement no. 956172 (xCTing). JS also acknowledges support from the Flemish Government under the "Onderzoeksprogramma Artificiële Intelligentie (AI) Vlaanderen" programme.

Appendix

Additional figures are provided in this section.

Fig. A.1 presents the original error percentage values for both the Nominal STL model and the Calibrated STL model, alongside a comparison with the real XCT scan results. The choice of surface model (the nominal STL model, the "calibrated" STL) significantly impacts simulation results, emphasizing the importance of using accurate and representative models in XCT simulations. The results demonstrate that using a calibrated STL model based on reference measurements produces simulations that more closely match real XCT scan behavior. Currently, our approach aims to estimate the deviation error as closely as possible to real XCT data, in order to isolate the individual physical effects. To achieve this efficiently, we applied a calibrated STL model. Notably, the error patterns in Figure A1 are similar for both the calibrated and nominal STL models, depending on the position of the cylinder hole within the volume (e.g., both show comparable color patterns with positive and negative errors in similar locations). However, the error magnitudes are higher in the nominal model (Nominal-STL simulation scale: $\approx$ 2.50–3.50), whereas the calibrated model (Calibrated-STL simulation scale: $\approx$ −0.75–0.25) produces values much closer to the real CT scan errors (Real CT scan scale: $\approx$ −0.60–0.20). In future work, we aim to reduce the need for high-quality reference measurements by incorporating iterative refinement steps that enable more accurate deviation estimation directly from the nominal STL model.

Fig. A.2 presents the original error percentage values for real XCT reconstructions, comparing results obtained using 120 and 1000 projections. Typically, a unified color-bar range should be applied across all cases for consistent comparison. However, in Figs. A.1 and A.2, individual color-bars were used for each case to more effectively illustrate the behavior of the deviations. However, in Figs. A.1 and A.2, we adjusted it to better illustrate the behavior of the deviations. As seen in Fig. A.1, the error behavior is similar for both the Nominal STL model and the Calibrated STL model; however, the error percentage is significantly higher in the simulations generated from the Nominal STL model. The color-coded bar fixed value ranges also presented in following figure for Fig. A.2.

Fig. A.3 compares the X-ray simulation against the real XCT image for a sample in raw data, showing a strong visual agreement between the two cross-sectional slices. The accompanying grey value profile quantitatively confirms this correspondence, with the orange (Real XCT) and blue (Simulation) lines closely tracing each other's dips and peaks along the marked red line. This high level of consistency demonstrates that the simulation accurately reproduces the grey value behavior observed in the real XCT data.

Data availability

Data will be made available on request.

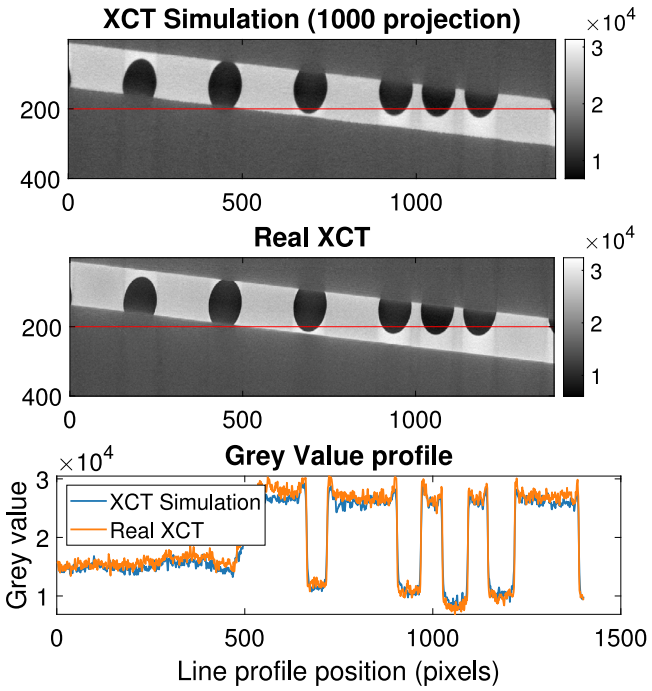

Fig. A.3. Comparison of XCT simulations 1000 projections against real XCT images. The top and middle rows show XCT simulations and real XCT images, respectively, while the bottom row displays grey value profiles along the marked red line.

References

[1] C. Heinzl, S. Stappen, STAR: Visual computing in materials science, Comput. Graph. Forum 36 (2017) 647–666.

[2] S. Wang, J. Ning, L. Zhu, Z. Yang, W. Yan, Y. Dun, P. Xue, P. Xu, S. Bose, A. Bandyopadhyay, Role of porosity defects in metal 3D printing: Formation mechanisms, impacts on properties and mitigation strategies, Mater. Today 59 (2022) 133–160.

[3] J.M. Sietins, W.H. Green, J.S. Jones, Material evaluation using X-ray computed tomography, in: Compr. Struct. Integr., 2nd Ed., Elsevier, Adelphi, Maryland and Greenbelt, Maryland, United States, 2022.

[4] Z. Al-Nabulsi, J.T. Mottram, M. Gillie, N. Kourra, M.A. Williams, Mechanical and X-ray computed tomography characterisation of a WAAM 3D printed steel plate for structural engineering applications, Constr. Build. Mater. 274 (2021) 121700.

[5] F. Zanini, N. Bonato, S. Carmignato, New experimental approach for local measurements of effective layer thickness, powder bed density and volumetric energy density to enhance metal laser powder bed fusion, Addit. Manuf. 93 (2024) 104432.

[6] H. Villarraga-Gómez, E.L. Herazo, S.T. Smith, X-ray computed tomography: from medical imaging to dimensional metrology, Precis. Eng. 60 (2019) 544–569.

[7] K. Oubellaouch, R. Pelaccia, N. Bonato, N. Bettoni, S. Carmignato, L. Orazi, L. Donati, B. Reggiani, Assessment of fiber orientation models predictability by comparison with X-ray μCT data in injection-molded short glass fiber-reinforced polyamide, Int. J. Adv. Manuf. Technol. 130 (2024) 4479–4492.

[8] B. Plank, M.G.R. Sause, J. Kastner, High-resolution X-ray computed tomography simulations of synthetically-generated volume porosity in continuous carbon fibre-reinforced polymer samples, Nondestruct. Test. Eval. 37 (5) (2022) 645–665.

[9] C. Heinzl, A. Amirkhanov, J. Kastner, Processing, analysis and visualization of CT data, in: Ind. X-Ray Comput. Tomogr., Springer, Cham, 2018, pp. 99–142.

[10] I. Holgado, N. Ortega, J.A. Yagüe-Fabra, S. Plaza, H. Villarraga-Gómez, Metrological evaluation and classification of porosity in metal additive manufacturing using X-ray computed tomography, Mater. Des. 254 (2025) 114057.

[11] L. Vásárhelyi, Z. Kónya, Á. Kukovecz, R. Vajtai, Microcomputed tomography–based characterization of advanced materials: a review, Mater. Today Adv. 8 (2020) 100084.

[12] L. Qing, H. Sun, Y. Zhang, R. Mu, M. Bi, Research progress on aligned fiber reinforced cement-based composites, Constr. Build. Mater. 363 (2023) 129578.

[13] R.M. Auenhammer, N. Jeppesen, L.P. Mikkelsen, V.A. Dahl, B.J. Blinzler, L.E. Asp, Robust numerical analysis of fibrous composites from X-ray computed tomography image data enabling low resolutions, Compos. Sci. Technol. 224 (2022) 109458.

[14] M. Yosifov, P. Weinberger, B. Plank, B. Fröhler, M. Hoeglinger, J. Kastner, C. Heinzl, Segmentation of pores in carbon fiber reinforced polymers using the U-net convolutional neural network, Acta Polytech. CTU Proc. 42 (2023) 87–93.

[15] B. Fröhler, J. Weissenböck, M. Schiwarth, J. Kastner, C. Heinzl, open_iA: A tool for processing and visual analysis of industrial computed tomography datasets, J. Open Source Softw. 4 (35) (2019) 1185.

[16] A. Heim, A. Gall, M. Waldner, E. Gröller, C. Heinzl, AccuStripes: Visual exploration and comparison of univariate data distributions using color and binning, Comput. Graph. 119 (2024) 103906.

[17] A. Tsamos, S. Evsevleev, R. Fioresi, F. Faglioni, G. Bruno, Synthetic data generation for automatic segmentation of X-ray computed tomography reconstructions of complex microstructures, J. Imaging 9 (2023) 22.

[18] M. Yosifov, M. Reiter, S. Heupl, C. Gusenbauer, B. Fröhler, R. Fernández-Gutiérrez, J. De Beenhouwer, J. Sijbers, J. Kastner, C. Heinzl, Probability of detection applied to X-ray inspection using numerical simulations, Nondestruct. Test. Eval. 37 (2022) 536–551.

[19] M. Yosifov, P. Weinberger, M. Reiter, B. Fröhler, J. De Beenhouwer, J. Sijbers, J. Kastner, C. Heinzl, Defect detectability analysis via probability of defect detection between traditional and deep learning methods in numerical simulations, E-J. Nondestruct. Test. 28 (2023).

[20] S. Carmignato, W. Dewulf, R. Leach (Eds.), Industrial X-ray Computed Tomography, Springer, Cham, 2018.

[21] A. Buratti, J. Bredemann, M. Pavan, R. Schmitt, S. Carmignato, Applications of CT for dimensional metrology, in: Ind. X-Ray Comput. Tomogr., Springer, Cham, 2018, pp. 333–369.

[22] F. Zanini, E. Sbettega, S. Carmignato, X-ray computed tomography for metal additive manufacturing: challenges and solutions for accuracy enhancement, Procedia CIRP 75 (2018) 114–118.

[23] V.D. Ingenieure, Computed tomography in dimensional measurement—determination of the uncertainty of measurement and the test process suitability of coordinate measurement systems with CT sensors, VDI/VDE 2630-2.1, Düsseldorf, 2015.

[24] E. Savio, H.N. Hansen, L. De Chiffre, Approaches to the calibration of freeform artefacts on coordinate measuring machines, CIRP Ann. 51 (2002) 433–436.

[25] F. Zanini, S. Carmignato, E. Savio, Two different experimental approaches for the uncertainty determination of X-ray computed tomography dimensional measurements on lattice structures, CIRP J. Manuf. Sci. Technol. 47 (2023) 205–214.

[26] M. Ferrucci, E. Ametova, Charting the course towards dimensional measurement traceability by X-ray computed tomography, Meas. Sci. Technol. 32 (9) (2021) 9.

[27] W. Dewulf, H. Bosse, S. Carmignato, R. Leach, Advances in the metrological traceability and performance of X-ray computed tomography, CIRP Ann. 71 (2022) 693–716.

[28] H. Villarraga-Gómez, J.D. Thousand, S.T. Smith, Empirical approaches to uncertainty analysis of X-ray computed tomography measurements: A review with examples, Precis. Eng. 64 (2020) 249–268.

[29] Joint Committee for Guides in Metrology, International Vocabulary of Metrology – Basic and General Concepts and Associated Terms, 3rd ed., VIM, 2012, https://www.bipm.org/documents/20126/2071204/JCGM_200_2012.pdf.

[30] Joint Committee for Guides in Metrology, JCGM 100: Evaluation of Measurement Data—Guide to the Expression of Uncertainty in Measurement, 2008, No. JCGM 100.

[31] Joint Committee for Guides in Metrology, JCGM 101: Evaluation of Measurement Data—Supplement 1 to the 'Guide to the Expression of Uncertainty in Measurement'—Propagation of Distributions Using a Monte Carlo Method, 2008, No. JCGM 101.

[32] Joint Committee for Guides in Metrology, JCGM 102: Evaluation of Measurement Data—Supplement 2 to the "Guide to the Expression of Uncertainty in Measurement"—Extension to Any Number of Output Quantities, 2011, No. JCGM 102.

[33] F. Binder, B.A. Bircher, R. Laquai, A. Küng, C. Bellon, F. Meli, A. Deresch, U. Neuschaefer-Rube, T. Hausotte, Methodologies for model parameterization of virtual CTs for measurement uncertainty estimation, Meas. Sci. Technol. 33 (10) (2022) 104002.

[34] M. Braun, T. Reuter, C. Bellon, A. Orth, M. Bartscher, K. Li, S. Kasperl, K. Kirschbaum, T. Hausotte, Simulation of a real dimensional CT measurement study using a calibrated aluminum specimen, E-J. Nondestruct. Test. 30 (8) (2025) International Symposium on Digital Industrial Radiology and Computed Tomography (DIR 2025), Paris, France, 1–3 Jul 2025.

[35] T. Reuter, F. Borges de Oliveira, C. Abt, F. Ballach, M. Bartscher, C. Bellon, F. Dennerlein, P. Fuchs, O. Günnewig, T. Hausotte, et al., Introduction to "realistic simulation of real CT systems with a basic-qualified simulation software—CTSimU2", in: E-J. Nondestruct. Test., 2023, 12th Conference of Industrial Computed Tomography (iCT 2023).

[36] A. Orth, C. Bellon, M. Braun, K. Li, T. Reuter, M. Bartscher, S. Kasperl, T. Hausotte, Realistische simulation von Röntgencomputertomografie-systemen, 2025, DGZfP.

[37] International Organization for Standardization (ISO), ISO/TS 15530-3: Geometrical Product Specifications (GPS)—Coordinate Measuring Machines (Cmm): technique for Determining the Uncertainty of Measurement—Part 3: use of Calibrated Workpieces or Measurement Standards, 2011, No. ISO/TS 15530-3.
[38] P. Müller, J. Hiller, Y. Dai, J.L. Andreasen, H.N. Hansen, L. de Chiffre, Estimation of measurement uncertainties in X-ray computed tomography metrology using the substitution method, CIRP J. Manuf. Sci. Technol. 7 (3) (2014) 222–232.
[39] J. Hiller, P. Hornberger, Measurement accuracy in X-ray computed tomography metrology: toward a systematic analysis of interference effects in tomographic imaging, Precis. Eng. 45 (2016) 18–32.
[40] W. Cao, T. Sun, G. Kerckhofs, G. Fardell, B. Price, W. Dewulf, A simulation-based study on the influence of the X-ray spectrum on the performance of multi-material beam hardening correction algorithms, Meas. Sci. Technol. 29 (2018) 095002.
[41] M. Ferrucci, P. Heřmánek, E. Ametova, S. Carmignato, W. Dewulf, Measurement of the X-ray computed tomography instrument geometry by minimization of reprojection errors—Implementation on simulated data, Precis. Eng. 54 (2018) 7–20.
[42] E. Hüllermeier, W. Waegeman, Aleatoric and epistemic uncertainty in machine learning: an introduction to concepts and methods, Mach. Learn. 110 (2021) 457–506.
[43] S. Yang, T. Fevens, Uncertainty quantification and estimation in medical image classification, in: Artif. Neural Netw. Mach. Learn. – ICANN 2021, Lect. Notes Comput. Sci., 2021, pp. 669–681.
[44] Y. Gal, Z. Ghahramani, Dropout as a Bayesian approximation: Representing model uncertainty in deep learning, in: Proc. 33rd Int. Conf. Mach. Learn., Proc. Mach. Learn. Res., 2016, pp. 1050–1059.
[45] F. Zanini, N. Bonato, D. Pentucci, S. Carmignato, Investigating the effects of machine learning generalization for enhancing accuracy in fast X-ray computed tomography for industrial metrology, CIRP Ann. 74 (2025).
[46] J.P. Kruth, M. Bartscher, S. Carmignato, R. Schmitt, L. De Chiffre, A. Weckenmann, Computed tomography for dimensional metrology, CIRP Ann. 60 (2011) 821–842.
[47] M. Reiter, S. Kasperl, C. Kuhn, M. Erler, D. Weiß, C. Heinzl, C. Gusenbauer, J. Kastner, Evaluation of transmission based image quality optimisation for X-ray computed tomography, in: 4th Conf. Ind. Comput. Tomogr., ICT, 2012.
[48] J. Makarov, M. Basting, R. Schielein, M. Schmitt, D. Kabitzky, F. Sukowski, V. Voland-Salamon, Computed tomography with or without radiation, E-J. Nondestruct. Test. 28 (2023).
[49] W. van Aarle, W.J. Palenstijn, J. Cant, E. Janssens, F. Bleichrodt, A. Dabravolski, J. De Beenhouwer, K.J. Batenburg, J. Sijbers, Fast and flexible X-ray tomography using the ASTRA toolbox, Opt. Express 24 (2016) 25129–25147.
[50] C. Bellon, A. Deresch, C. Gollwitzer, G. Jaenisch, Radiographic simulator artist: Version 2, in: 18th World Conf. Nondestruct. Test., E-J. Nondestruct. Test., 2012.
[51] M. Reiter, M. Erler, C. Kuhn, C. Gusenbauer, J. Kastner, SimCT: a simulation tool for X-ray imaging, in: 6th Conf. Ind. Comput. Tomogr., ICT, 2016.
[52] T. Reuter, F. Borges de Oliveira, C. Abt, F. Ballach, M. Bartscher, C. Bellon, F. Dennerlein, P. Fuchs, O. Günnewig, T. Hausotte, et al., Introduction to “realistic simulation of real CT systems with a basic-qualified simulation software - CTSimU2”, in: 12th Conf. Ind. Comput. Tomogr. (ICT) 2023, E-J. Nondestruct. Test., 2023.
[53] S. Su, N. Dai, X. Cheng, et al., A study on factors influencing the accuracy evaluation of dimensional X-ray computed tomography with multi-sphere standards, Int. J. Precis. Eng. Manuf. 21 (2020) 649–661.
[54] H. Villarraga-Gómez, C. Lee, S.T. Smith, Dimensional metrology with X-ray CT: A comparison with CMM measurements on internal features and compliant structures, Precis. Eng. 51 (2018) 291–307.
[55] Y. Tan, K. Kiekens, F. Welkenhuyzen, J. Kruth, W. Dewulf, Beam hardening correction and its influence on the measurement accuracy and repeatability for CT dimensional metrology applications, in: 4th Conf. Ind. Comput. Tomogr., ICT, 2012, pp. 19–21.
[56] J. Hiller, M. Maisl, L.M. Reindl, Physical characterization and performance evaluation of an X-ray micro-computed tomography system for dimensional metrology applications, Meas. Sci. Technol. 23 (2012) 085404.
[57] M. Reiter, D. Weiß, C. Gusenbauer, M. Erler, C. Kuhn, S. Kasperl, J. Kastner, Evaluation of a histogram-based image quality measure for X-ray computed tomography, in: 5th Conf. Ind. Comput. Tomogr. (ICT) 2014, 2014.
[58] L. Feldkamp, L. Davis, J. Kress, Practical cone-beam algorithm, J. Opt. Soc. Amer. A 1 (1984) 612–619.
[59] Y.-K. Park, G.C. Sharp, Gain correction for an X-ray imaging system with a movable flat panel detector and intrinsic localization crosshair, Technol. Cancer Res. Treat. 15 (2016) 387–395.
[60] J.J. Lifton, R.S. Bradley, A. McNeil, S. Titarenko, P.J. Withers, The influence of focal spot size on the measurement accuracy of X-ray computed tomography for dimensional metrology, NDT & E Int. 75 (2015) 23–31.
[61] J. Hiller, P. Hornberger, Measurement accuracy in X-ray computed tomography metrology: Toward a systematic analysis of interference effects in tomographic imaging, Precis. Eng. 45 (2016) 222–231.
[62] A. Kraemer, G. Lanza, Methodology for the evaluation of CT image quality in dimensional metrology, Proc. the 6th Conf. Ind. Comput. Tomogr. (ICT 2016) (2016).
[63] J.J. Lifton, A.A. Malcolm, J.W. McBride, A simulation-based study on the influence of beam hardening in X-ray computed tomography for dimensional metrology, Insight - Non-Destructive Test. Cond. Monit. 56 (11) (2014) 605–611.
[64] A. Kraemer, M. Schoggl, G. Lanza, Influence of noise on surface determination in industrial X-ray computed tomography, Meas. Sci. Technol. 31 (12) (2020) 125401.
[65] J.-P. Kruth, M. Bartscher, S. Carmignato, R. Schmitt, L. De Chiffre, A. Weckenmann, Computed tomography for dimensional metrology, CIRP Ann 60 (2) (2011) 821–842.
[66] W. Dewulf, K. Kiekens, Y. Tan, F. Welkenhuyzen, J.-P. Kruth, Uncertainty Determination and Quantification in Dimensional Metrology Using Computed Tomography, Tech. rep, KU Leuven, 2014, Related to multiple publications on CT error sources and uncertainty.
[67] M. Bartscher, O. Sato, F. Härtig, U. Neuschaefer-Rube, Current state of standardization in the field of dimensional computed tomography, Meas. Sci. Technol. 25 (6) (2014) 064013.
[68] Z. Wang, A.C. Bovik, H.R. Sheikh, E.P. Simoncelli, Image quality assessment: from error visibility to structural similarity, IEEE Trans. Image Process. 13 (2004) 600–612.
[69] H.R. Sheikh, M.F. Sabir, A.C. Bovik, A statistical evaluation of recent full reference image quality assessment algorithms, IEEE Trans. Image Process. 15 (2006) 3440–3451.
[70] T.J. Sørensen, A method of establishing groups of equal amplitude in plant sociology based on similarity of species and its application to analyses of the vegetation on danish commons, K. Dan. Vidensk. Selsk. Biol. Skr. 5 (1948) 1–34.
[71] H. Villarraga-Gómez, S.T. Smith, Effect of the number of projections on dimensional measurements with X-ray computed tomography, Precis. Eng. 66 (2020) 445–456.
[72] J. Sun, X. Li, M. Zhang, Y. Wang, The realization of fast X-ray computed tomography using a limited number of projection images for dimensional metrology, 2023, ArXiv Preprint arXiv:2305.10129.
[73] C. Orgeldinger, M. Wohlgemuth, K. Müller, T. Hausotte, Towards efficient application-dependent dimensional measurements with computed tomography: optimized reduction of measurement duration using continuous scan mode, J. Sensors Sens. Syst. 11 (2022) 219–232.
[74] F. Binder, B.A. Bircher, R. Laquai, A. Küng, C. Bellon, F. Meli, A. Deresch, U. Neuschaefer-Rube, T. Hausotte, Measurement science and technology, volume 33, number 10, Meas. Sci. Technol. 33 (10) (2022) 104002.
[75] H. Villarraga-Gómez, E.P. Morse, S.T. Smith, Assessing the effect of penetration length variations on dimensional measurements with X-ray computed tomography, Precis. Eng. 79 (2023) 146–163.
[76] H. Villarraga-Gómez, A. Amirkhanov, C. Heinzl, S.T. Smith, Assessing the effect of sample orientation on dimensional X-ray computed tomography through experimental and simulated data, Measurement 178 (2021) 109343.
[77] C. Rossides, H. Towsyfyan, A. Biguri, H. Deyhle, R. Lindroos, M. Mavrogordato, R. Boardman, W. Sun, T. Blumensath, Effects of fast X-ray cone-beam tomographic measurement on dimensional metrology, Metrologia 59 (4) (2022) 044003.
[78] M. Bartscher, O. Sato, J. Illemann, U. Neuschaefer-Rube, F. Härtig, Coordinate metrology using computed tomography systems – an overview of ptb’s activities with a focus on standardization, in: Industrial CT Scanning German-Austrian-Danish Workshop, Munich, Germany, 2013, 24–25 Oct 2013.
[79] E. Sbettega, Accuracy Enhancement of Industrial X-ray Computed Tomography for Dimensional Metrology (Ph.D. thesis), Università degli Studi di Padova, 2020.
[80] J. Rathore, C. Vienne, Y. Quinsat, C. Tournier, Influence of resolution on the X-ray CT-based measurements of metallic AM lattice structures, Weld. the World 64 (2019) 1367–1376.
[81] S. Brisard, M. Serdar, P.J. Monteiro, Multiscale X-ray tomography of cementitious materials: A review, Cem. Concr. Res. 128 (2020) 105824.